DEVELOPMENT OF Ru^0/MO_2 (M = Ti, Zr, Hf, Ce) CATALYSTS FOR ELECTROCATALYTIC HYDROGEN PRODUCTION FROM WATER SPLITTING

A THESIS SUBMITTED TO
THE GRADUATE SCHOOL OF NATURAL AND APPLIED SCIENCES
OF
MIDDLE EAST TECHNICAL UNIVERSITY

BY

ELİF DEMİR

IN PARTIAL FULFILLMENT OF THE REQUIREMENTS
FOR
THE DEGREE OF MASTER OF SCIENCE
IN
CHEMISTRY

AUGUST 2017

Approval of the thesis:

DEVELOPMENT OF Ru^0/MO_2 (M = Ti, Zr, Hf, Ce) CATALYSTS FOR ELECTROCATALYTIC HYDROGEN PRODUCTION FROM WATER SPLITTING

submitted by **ELİF DEMİR** in partial fulfillment of the requirements for the degree of **Master of Science in Chemistry Department, Middle East Technical University** by,

Prof. Dr. Gülbin Dural Ünver
Dean, Graduate School of **Natural and Applied Sciences** _____

Prof. Dr. Cihangir Tanyeli
Head of Department, **Chemistry** _____

Prof. Dr. Ahmet M. Önal
Supervisor, **Chemistry Dept.**, METU _____

Examining Committee Members:

Prof. Dr. Gülsün Gökağaç
Chemistry Dept., METU _____

Prof. Dr. Ahmet M. Önal
Chemistry Dept., METU _____

Prof. Dr. Ali Çırpan
Chemistry Dept., METU _____

Assoc. Prof. Dr. Emren Nalbant Esentürk
Chemistry Dept., METU _____

Asst. Prof. Dr. Buket Çarbaş
Dept. of Energy Systems Engineering, Karamanoğlu Mehmetbey University _____

Date: **16.08.2017**

I hereby declare that all information in this document has been obtained and presented in accordance with academic rules and ethical conduct. I also declare that, as required by these rules and conduct, I have fully cited and referenced all materials and results that are not original to this work.

Name, Last name: Elif Demir

Signature:

ABSTRACT

DEVELOPMENT OF Ru^0/MO_2 (M = Ti, Zr, Hf, Ce) CATALYSTS FOR ELECTROCATALYTIC HYDROGEN PRODUCTION FROM WATER SPLITTING

Demir, Elif

M.S., Department of Chemistry
Supervisor: Prof. Dr. Ahmet M. Önal

August 2017, 74 pages

In this study, Ru^0/MO_2 catalysts were prepared by reduction of ruthenium(III) chloride on different types of metal oxides, which were TiO_2, ZrO_2, CeO_2 and HfO_2, then catalysts were loaded on glassy carbon (GC) electrodes at same mass loading level, and used as electrocatalysts in 0.5 M H_2SO_4 solution for hydrogen evolution reaction (HER). Characterization of prepared catalysts were done by using transmission electron microscopy (TEM), energy dispersive X-ray (EDX), X-ray diffraction (XRD) spectroscopy and X-ray photoelectron spectroscopy (XPS), also, loading level of these catalysts were investigated by using inductively coupled plasma-optical emission spectrometry (ICP-OES)**.** Electrochemical behavior of the modified glassy carbon electrodes and their electrocatalytic activity towards the hydrogen evolution during water electrolysis was investigated in acidic solution (0.5 M H_2SO_4) at room temperature by linear sweep voltammetry (LSV), cyclic voltammetry (CV), potentiostatic electrochemical impedance spectroscopy (EIS) and constant potential electrolysis. Among the Ru^0/MO_2 modified GC electrodes, Ru^0/CeO_2 modified GCE was found to be better for HER in terms of onset potentials, current density at a defined overpotential, exchange current densities and Tafel slopes.

To investigate the amount of Ruthenium on the electrocatalytic effect, different loading levels of Ru^0/CeO_2-GC electrodes were prepared and analyzed towards hydrogen evolution reaction during water electrolysis. The glassy carbon electrode modified by Ru^0/CeO_2 with a ruthenium loading of 1.86% wt. provided an outstanding electrochemical activity with a high exchange current density of 0.67 $mA.cm^{-2}$, low overpotential of (η) 47 mV at j = 10 $mA.cm^{-2}$ and small Tafel slope of 41 $mV.dec^{-1}$.

Furthermore, electrocatalytic activity of Ru^0/MO_2 modified GCEs towards the oxygen evolution during water electrolysis was investigated in 0.5 M KOH solution. Ru^0/CeO_2 (1.86% wt. Ru)-GC electrode was found to exhibit better electrocatalytic activity towards OER.

Keywords: Ruthenium (Ru^0) nanoparticles; Catalysts; Water electrolysis; Hydrogen generation; Oxygen generation; Bifunctional/Dual Catalyst

ÖZ

SUYUN ELEKTROLİZİNDEN ELEKTROKATALİTİK HİDROJEN ÜRETİMİ İÇİN Ru^0/MO_2 (M = Ti, Zr, Hf, Ce) KATALİZÖRLERİN GELİŞTİRİLMESİ

Demir, Elif

Yüksek Lisans, Kimya Bölümü

Tez Yöneticisi: Prof. Dr. Ahmet M. Önal

Ağustos 2017, 74 sayfa

Değişik metal oksit yüzeyinde rutenyum(III) klorürürün indirgenmesi ile hazırlanan Ru^0/MO_2 (M = Ti, Zr, Hf, Ce) katalizörleri camsı karbon (GC) elektrotlar üzerine aynı kütle yüklemesinde konularak, 0.5 M H_2SO_4 içeren sulu çözeltiden hidrojen salımı tepkimesi (HER) için elektrokatalizör olarak denendi. Hazırlanan katalizörlerin karakterizasyonu transmisyon elektron mikroskopisi (TEM), enerji dağılımlı X-ray (EDX), X-ışını kırınım spektroskopisi (XRD) ve X-ışını fotoelektron spektroskopisi (XPS) kullanılarak yapıldı, katalizörlerin yükleme seviyeleri ise indüktif eşleşmiş plazma-optik emisyon spektrometresi (ICP-OES) kullanılarak araştırıldı. Modifiye edilmiş camsı karbon elektrotların elektrokimyasal davranışları ve bunların suyun elektrolizi sırasında hidrojen salımına olan elektrokatalitik aktiviteleri, asidik çözeltide (0.5 M H_2SO_4), oda sıcaklığında doğrusal süpürme voltametrisi (LSV), dönüşümlü voltametri (CV), potentiyostatik elektrokimyasal impedans spektroskopi (EIS) ve sabit potansiyel elektrolizi ile analiz edildi. Ru^0/MO_2 ile modifiye edilmiş GC elektrotları ile elde edilen sonuçlar, başlama potansiyeli, belirlenen potansiyellerdeki akım yoğunluğu, değişim akım yoğunluğu ve Tafel eğimleri kıyaslandığında HER için Ru^0/CeO_2 modifiye GC elektrodunun diğerlerinden daha iyi olduğu görüldü.

Ruthenyum miktarının elektrokatalitik etkiye katkısını incelemek amacı ile, Ru^0/CeO_2-GC elektrotları farklı yüklenme seviyelerinde hazırlandı ve suyun elektrolizi sırasında hidrojen salımı reaksiyonuna karşı analiz edildi. Kütlece %1.86 Ru yüklü Ru^0/CeO_2 ile modifiye edilmiş camsı karbon elektrodun; yüksek değişim akım yoğunluğuna (j_0 = 0.67 $mA.cm^{-2}$), (j)= 10 $mA.cm^{-2}$ akım yoğunluğuna ulaşmak için düşük potensiyele (η= 47 mV) ve görece olarak daha küçük Tafel eğimine (41 $mV.dec^{-1}$) sahip üstün bir elektrokimyasal aktivite sağladığı saptandı.

Bunlara ek olarak, Ru^0/MO_2 ile modifiye edilmiş camsı karbon elektrotları, oksijen salımına yönelik elektrokatalitik etkinlikleri 0.5 M KOH çözeltisi içinde incelendi. Elde edilen sonuçlardan Ru^0/CeO_2 (kütlece %1.86 Ru)-GC elektrotunun, OER'ye karşı en iyi katalitik aktiviteye sahip olduğu bulundu.

Anahtar Kelimeler: Ruthenyum(0) nanopartikülleri; Katalizörler; Hidrojen salımı; Oksijen salımı; Çift fonksiyonlu katalizör

To my beloved family,

ACKNOWLEDGEMENTS

First of all, I would like to express my sincere thanks to my supervisor Prof. Dr. Ahmet M. ÖNAL for his priceless support, guidance and encouragement during my graduate studies. I am deeply honored to have a chance to work with him, and to be member of his highly respected research group.

I would like to express my appreciation and thanks to Prof. Dr. Saim ÖZKAR for his guidance, support and valuable ideas during the research.

I wish to express my appreciation to Dr. Serdar AKBAYRAK for his support, answering my questions about inorganic part of my research with patience.

I would like to thank Prof. Dr. Ayşen YILMAZ for XRD measurements.

I would also like to thank my lab-mates Deniz ÇAKAL and Merve AKBAYRAK for their friendship and providing enjoyful working environment.

I want to express my gratitude to my friends, who were always with me in good time and in bad times.

I thank Atılım University for providing me a nice working environment.

I would like to give my special thanks my fiancée Burak ARABACI for his love, patience, moral support, joy and encouragement in every moment of my life.

The last but not the least, my special appreciation and great gratitude is devoted to my dear parents Mustafa-Gülşan DEMİR and my brother Ekin DEMİR for their endless moral support and motivation. Without their encouragement and immeasurable sacrifice, I could never finish this journey.

TABLE OF CONTENTS

LIST OF FIGURES

FIGURES

LIST OF TABLES

TABLES

LIST OF ABBREVIATIONS

TEM: Transmission Electron Microscopy

EDX: Energy Dispersive X-ray

ICP-OES: Inductively Coupled Plasma - Optical Emission Spectroscopy

XRD: X-Ray Powder Diffraction

GCE: Glassy Carbon Electrode

Pt: Platinum

RHE: Reverse Hydrogen Electrode

NHE: Normal Hydrogen Electrode

NPs: Nanoparticles

PBS: Phosphate Buffer Saline

Ru^0/TiO_2: Ruthenium(0) Nanoparticles Supported on Titanium dioxide

Ru^0/ZrO_2: Ruthenium(0) Nanoparticles Supported on Zirconium dioxide

Ru^0/HfO_2: Ruthenium(0) Nanoparticles Supported on Hafnia dioxide

Ru^0/CeO_2: Ruthenium(0) Nanoparticles Supported on Ceria dioxide

TOF: Turnover Frequency Number

η: Overpotential

E: Potential

j_0: Exchange Current Density

HER: Hydrogen Evolution Reaction

OER: Oxygen Evolution Reaction

CHAPTER 1

INTRODUCTION

Since beginning of social life, energy has become indispensable for humanity due to development of society, production and industrialization. For centuries, humanity has constantly improved itself and has renewed its needs. In this process, the only requirement that does not change is energy and the World energy demand is increasing rapidly with modernization and industrialization. Therefore, the World energy sources are depleting so fast due to increasing consumption of fossil fuels such as, coal, oil and gas. Furthermore, the World temperature is increasing at an alarming rate and the amount of greenhouse gases are rising with excessive use of carbon based fossil fuels. Hence, searching for renewable energy sources as an alternative to fossil fuels is an attractive issue. During the past several decades, there have been countless investigations and developments in the areas of clean and renewable energy sources [1].

Hydrogen (H_2) is proposed to be a major energy resource for the future world [2]. H_2, one of the most abundant element in the earth's crust, can be found in fossil fuels, all plants, amino acids, proteins, carbohydrates and some other types of compounds. However, it does not exist as a free molecule in earth's atmosphere, and consequently, efficient and sustainable hydrogen production technologies are required. Therefore, hydrogen is not a primary source of energy, it must be extracted from primary energy sources such as water or hydrocarbons. Taking this information into account, it can be said that hydrogen is not a source of energy but is an energy carrier like electricity [3]. The implementation of H_2 as an energy carrier is covetable since H_2 has the highest energy density per unit mass.

Furthermore, when it is transformed into electricity in a fuel cell or combusted in an engine, it produces only one product, water. On the other hand, carbon-based fuels produce water and carbon dioxide (CO_2) [4].

The aim of this study is to prepare and characterize ruthenium(0) nanoparticles supported on different reducible oxides such as ceria (CeO_2), titania (TiO_2), hafnia (HfO_2) and zirconia (ZrO_2) and to investigate their applicability in modifying GC electrodes to be used as electrocatalyst during electrolysis of water. Ruthenium(0) nanoparticles supported on reducible oxides were characterized by ICP-OES, EDX, TEM and XPS. Ru^0/MO_2 (M = Ti, Zr, Hf, Ce) were used to modify glassy carbon (GC) electrodes at same mass loading level (≈ 0.197 mg/cm^2) by drop casting. Finally, the effect of different types of metal oxides and loading level were investigated in hydrogen evolution reaction, HER, and oxygen evolution reaction, OER, by recording the polarization curves for the modified electrodes in acidic and alkaline solutions.

1.1. Use of Transition Metal Nanoparticles as Catalysts

1.1.1. Catalysts

Substances which accelerate the reaction by changing the reaction path with lower energy barrier and do not undergo a change in the chemical structure after the reaction are known as catalysts. They not only increase the reaction rate but also, as shown in Figure 1 lower the activation energy (E_a). Furthermore, reactions in the presence of a suitable catalyst proceed in different pathway from reaction without catalyst. Thus, reactions occur faster at lower temperatures and pressures with high selectivity. During the reaction, catalyst makes a bond with reactants (i.e. adsorption) to form particular product, which detaches itself from the catalyst (i.e. desorption) so at the end of reaction catalyst can be obtained as unaltered and ready to reuse for other reactions.
Catalysts with high selectivity are used as an aid to reduce energy consumption in the chemical industry and are used to perform processes such as waste disposal and product separation. Since catalysts increase the efficiency and the rate of reaction and

provides high selectivity, they are important for industrial processes such as producing fuels, fertilizers, medicines, textiles and so on [5].

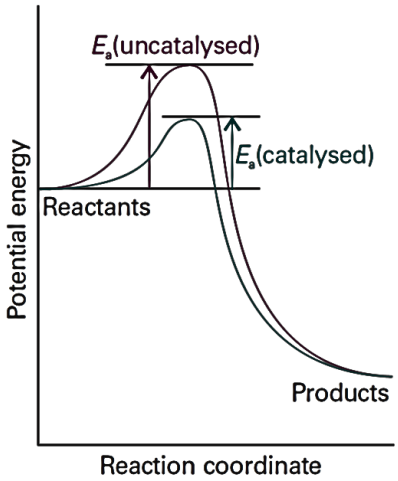

Figure 1. Energy diagram of an exothermic chemical reaction illustrating the different path with a lower activation energy with catalyst [5].

1.1.2. Classification of Catalysts

Catalysts are examined under three main categories such as; homogeneous catalysts, heterogeneous catalysts and biocatalysts.

1.1.2.1. Homogeneous Catalyst

Homogeneous catalysts are those substances which are in the same phase as the reactants and homogeneously mix in each other. Homogeneous catalysts consist of well-defined chemical or coordination compounds. Bronsted, Lewis acid and base, metal complexes, metal ions, organometallic complexes, organic molecules and enzymes are the examples of homogeneous catalysts. In addition to this, they react very quickly and provide a good conversion rate per catalyst molecule. One disadvantage of using homogeneous catalyst is separation of catalyst from the reaction mixture when the reaction is over. Homogeneous catalysts are generally used in the synthesis of pharmaceuticals and foods [6].

1.1.2.2. Heterogeneous Catalyst

Heterogeneous catalysts are those substances which are in the different phase as the reactants. Generally, catalysts are in the solid form and reactants are in the form of liquids and gases. Heterogeneous catalysts are commonly used for many industrial processes. The most important properties of these catalysts are that they are stable even at very high temperatures and can easily be recovered from the reaction medium because they are present in different phase from reagents. Metals, semiconductors, insulating materials and solid acids are generally used as heterogeneous catalysts. Compared with homogeneous catalysts, preparation of heterogeneous catalysts is simpler and cheaper because there is no limitation in terms of solvent. Consequently, heterogeneous catalysts are mostly preferred due to reusability, low price and stability [7].

1.1.2.3. Biocatalysts

Enzymes, which are biological catalysts, are very specific and can have a dramatic effect on the reactions that they control. Most enzymes are proteins, which are formed from amino acid monomers. For example, the enzyme catalase reduces the activation energy for the decomposition of hydrogen peroxide to 8 $kJ.mol^{-1}$, corresponding to an acceleration of the reaction by a factor of 1015 at 298 K [5].

1.1.3. Applications of Transition Metal Nanoparticles as Catalysis

It is known that intrinsic properties of materials and properties of nanoparticles remarkably change with particle size. Several reports have explained that transition metal nanoparticles are more active catalyst than their bulk-counterparts in a variety of reactions because they have larger surface area that provides a large number of potentially active sites. The proportion of surface atoms, active centers for catalytic elementary processes, increases with decreasing particle size and makes the metal nanocparticles more active catalysts as compared to their bulk counterparts. Therefore, transition metal nanoparticles are important as catalysts since they imitate the metal surface activation and catalysis at the nanoscale. For this reason, they have a wide range of applications as catalysts in chemical reactions and provide significant

economic and environmental improvements in the synthesis of the fine chemicals [8]. There are many reactions in which transition metals nanoparticles are used as catalysts, for instance, Suziki [9], hydrogenations [10], Mizoroki-Heck coupling [11], hydrogenolysis [12], oxidation of alcohols [13], hydrosilations [14], catalytic reforming reaction [15].

1.1.4. Preparation of Transition Metal Nanoparticles

Reproducible synthesis of monodispersed metal NPs with narrow size distribution is one of the most important tasks in the synthesis metal NPs. The term "monodisperse" means that size of metal NPs deviate less than 10% from the average value. A deviation of about 20% from the mean particle size is defined as "narrow size distribution" [16]. Transition metal NPs are synthesized by using two approaches: "top down" and "bottom up" [17]. Top down approach is a physical method in which macro sized, bulk metal is split into small pieces (nanometer-sized) by using physical forces such as, milling and grinding. Synthesis of monodispersed nanoparticles is difficult thus, broad size distribution (>10 nm) of metal NPs can be obtained. Furthermore, the particles cannot be synthesized reproducibly; hence, catalytic activity is also irreproducible. On the other hand, bottom up approach is a chemical method which is most widely used to prepare monodisperse metal NPs. In this approach, starting materials are atoms or molecules (bottom) which react under chemical or physical circumstances to generate metal NPs by the reduction treatment [18]. Colloidal metal NPs are generally synthesized by the chemical reduction of metal salts dissolved in a suitable solvent. The factors that determines the particle size of metal NPs in the chemical synthesis are the metal salt itself, solvent, reducing and stabilizing agents together with temperature at which the process is conducted. Moreover, there are some different chemical approaches to prepare transition metal NPs; for instance, thermal or photochemical decomposition, electrochemical reduction, chemical reduction of transition metal complexes, metal vapor synthesis, sol-gel technique and so on.

1.1.5. Stabilization of Transition Metal Nanoparticles

Using transition metal NPs have some compelling points because they have tendency to aggregate to larger particles and ultimately they form bulk metal. Mostly, there is loss of properties linked with the colloidal particles of these metallic particles due to agglomeration. Therefore, they have relatively short lifetime and low stability. However, metal nanoparticles have been stabilized against agglomeration by using microporous or mesoporous materials with large surface; [19] for instance, carbon nanotubes [20], ceria [21], graphene [22] and metal organic framework [23]. There are three methods to prevent agglomeration: namely, electrostatic stabilization (known as DLVO type), steric stabilization and electrosteric stabilization [24].

1.1.5.1. Electrostatic Stabilization / DLVO Theory

Derjaugin, Landau, Verwey, and Overbeek developed electrostatic stabilization (DLVO) theory in 1940's for stabilizing nanoparticles. Briefly, the adsorption of the ions and its counter ions (coming from starting material) on the metal surface create an electrical double layer. This provides Columbic repulsion force, opposing van der Waals force, between individual particles, therefore, when they come to close each other, agglomeration of nanoparticles is prevented by this electrical double layer [25, 26]. Note that, electrostatic repulsion can prevent agglomeration when double layer electric potential is high enough (Figure 2) [27].

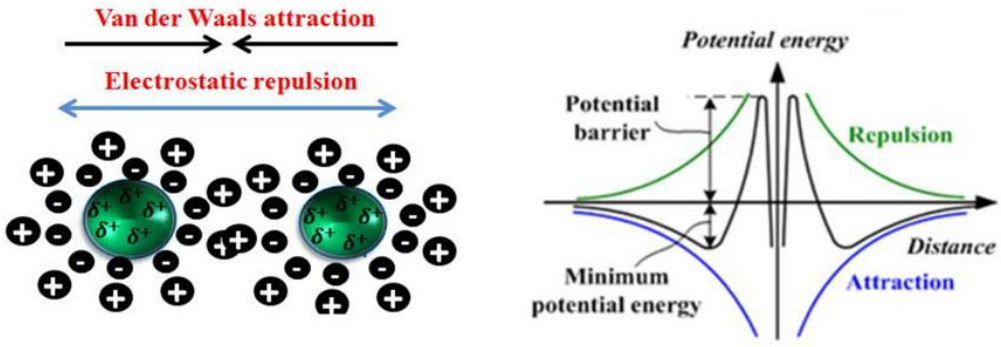

Figure 2. Schematic representation of the electrostatic stabilization between two particles and plot of energy versus distance between colloids [27].

1.1.5.2. Steric Stabilization

In this method, the surface of the transition metal nanoparticles is adsorbed by a polymer surfactant or long chain ligand to form a protective layer. Surfactants or ligands that surround the transition metal nanoparticles prevent close contact of transition metal nanoparticles to each other as illustrated in Figure 3 [28]. The polymer chains used to stabilize the transition metal nanoparticles exhibit steric interactions that transition metal nanoparticles form as they approach each other. The steric layers formed by adsorbing polymers prevent aggregation of transition metal nanoparticles and restrict the motion and conformations. Therefore, while entropy is going up, free energy is going down and monodisperse size metal nanoparticles can be synthesized [29].

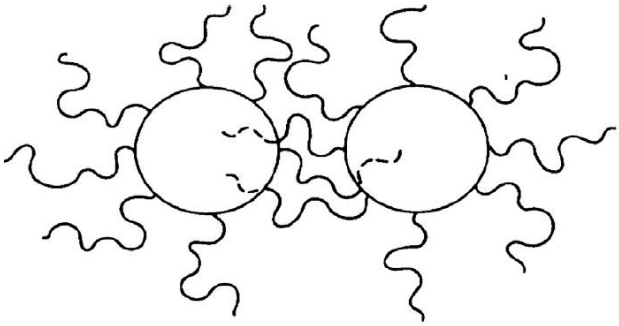

Figure 3. Schematic representation of the steric stabilization of transition metal nanoparticles [28].

1.1.5.3. Electrosteric Stabilization

To get thermodynamically stable metal nanoparticles, steric stabilization and electrostatic stabilization can be combined. In this method, the surface of the transition metal nanoparticles is adsorbed by surfactants such as polymers or long chain ligands to form a protective layer, and they must be in ionic form. Under favor of these ionic surfactants, steric effect and electrical double layer are formed. Therefore, due to steric layers and electrostatic repulsion, aggregation of transition metal nanoparticles is prevented when metal nanoparticles come close to each other as shown in Figure 4 [30].

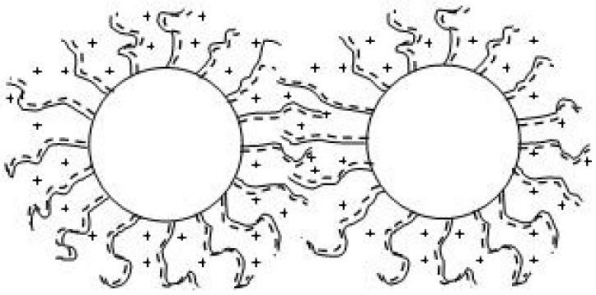

Figure 4. Schematic representation of the electrosteric stabilization of transition metal nanoparticles [30].

1.2. Hydrogen Economy

1.2.1. Global Energy Problems

Global energy need is supposed to increase in an alarming rate in the next decades due to increasing population and increasing living standards in worldwide. Today, all over the world major part of energy demand is supplied from fossil fuels, oil and coal. However, using fossil fuels causes a serious environmental problem known as global warming. Furthermore, these type of energy sources are non-renewable and World's energy resources are finite, so there will be insufficient resource for the future world. Moreover, releasing amount of carbon dioxide is increasing day by day due to consumption of carbon-based fuels, which causes global warming. In the near future, under the influence of the oil crisis and environmental problems, it is necessary to find alternative fuels to replace conventional petroleum-based fuels such as gasoline and diesel used in internal combustion engines. Therefore, there will be a need for new energy sources which are renewable and environmentally friendly because renewable energy sources are sustainable and also there are no waste products like CO_2 [31].

1.2.2. Hydrogen as an Energy Carrier

If an energy system uses hydrogen as an energy carrier, it is called as hydrogen economy. This process does not produce any greenhouse gas or CO_2 like fossil type energy sources. This is all to say, hydrogen energy is nontoxic and environmentally friendly. It supplies renewable and sustainable source [4]. Hydrogen is an energy system that can be locally produced, transported easily and safely everywhere with little energy loss during transport. Hydrogen energy is used in many types of reaction such as catalytic hydrogenation (ammonia synthesis, vegetable oil hardening, fatty acids, alcohol, methyl alcohol synthesis, drug production etc.), metallurgy (tungsten and molybdenum alloy, reduction material, preparing metal hydride etc.) and as a fuel (rockets, welding flame, metal heat combination, electricity production etc.) [32].

In addition to this, hydrogen can be better stored than electricity and transported over long distances. This feature allows hydrogen to be used as fuel in aircraft and motor vehicles. Also, hydrogen has the ability to obtain higher power than the gasoline because of its physical and chemical state and its positive effects on the environment make hydrogen an important alternative fuel. Although hydrogen has been used as a fuel, for motor vehicles, since 1920s however, some factors limited its use as a fuel. They mainly include the economic reasons and mismatch of traditional motor and present energy systems. Nevertheless, taking into account of environmental problems in the case of continuing use of fossil fuels as an energy source, hydrogen should be produced from clean energy sources [33].

As mentioned, there is a need for a renewable, clean fuel that is compatible with the ecological balance, both for the environment and for our energy needs. Using hydrogen as an energy carrier may be the solution of world's energy problem. Due to increasing energy requirements, intensive research and development activities are being carried out on hydrogen energy in recent years [34].

1.2.3. Hydrogen Production Techniques

Hydrogen does not exist as a free molecule in earth's atmosphere, and consequently, efficient and sustainable hydrogen production technologies are required. Presently, more than 44.5 million tons' hydrogen (or 500 billion cubic meters) are produced annually worldwide and most of the produced hydrogen consumed for industrial purposes such as treating metals, producing ammonia for fertilizers, refining petroleum and so on [35]. There are several methods for hydrogen production from renewable energy source and some of them are shown in Figure 5 [36].

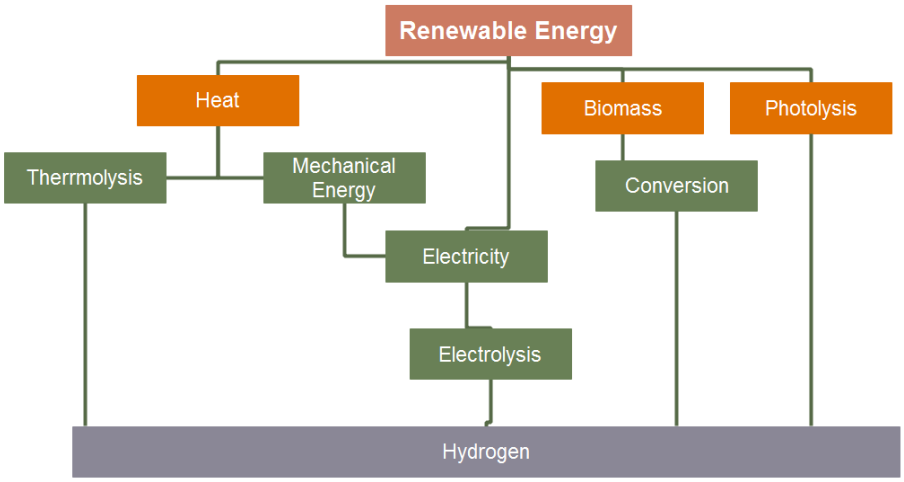

Figure 5. Sustainable pathways for hydrogen production from renewable energy sources [36].

1.2.3.1. Fossil Fuels

Fossil fuels are the oldest but the most widely used energy sources. It is used for various purposes as a raw material in transportation, heating, electricity, industrial applications and chemical industries. Fossil fuels are mixture of hydrocarbons that have been formed over a period of millions of years by the decaying of biomass. Petroleum and its derivatives, coal and oil are among the most commonly used fossil fuels. Nowadays, large quantities of hydrogen (more than 95%) used in industry are obtained from steam methane reforming and coal gasification which are fossil fuels—

the finite and nonrenewable resource. At the end of these production processes, CO_2 and H_2 are formed. Reactants and products of these hydrogen production techniques are shown in Table 1. As it is seen from the Table, these hydrogen production techniques violate our original goal—reducing global warming and air pollution by employing hydrogen energy [3].

Table 1. Fossil fuel based hydrogen production techniques.

Technology	Process
Steam Methane Reforming	$CH_4 + 2H_2O \rightarrow 4H_2 + CO_2$
Coal Gasification	$C + 2H_2O \rightarrow 2H_2 + CO_2$

1.2.3.2. Photochemical Hydrogen Production

For this type of hydrogen production technique, the anode or cathode of the light absorbing semiconducting material, or both, may be included in the electrochemical cell. When a semiconductor is exposed to a high-energy light source, the electrons in the valence band are stimulated to pass to an upper energy level (the conduction band) and leave electron holes in the valence band. Water electrolysis can be done by force of these photochemically created electrons and holes. In other words, while the electrons in the conduction band carry out the hydrogen reduction reaction of water, the electron holes in the valence band carry out the oxidation reaction of oxygen in the water.

It is one of the most environmentally friendly method for hydrogen production because water directly splits into hydrogen and oxygen by UV (ultraviolet) light coming from sunlight. Even though UV light have enough energy to directly separate water, only a fraction of it can reach to the earth's surface, as they are held in large quantities by the ozone layer in the atmosphere. The fact that UV light, which is harmful to all living things, actually passes through the thinner ozone easily as a means of boosting the photochemical process, poses a serious threat to our world. However, for the photochemical method, it is necessary to enhance the absorption of radiation or to

increase the absorption by water. For this reason, the UV effect is enhanced by adding some minerals and metals into the water with a set of solar light condensing devices [37].

1.2.3.3. Thermochemical Hydrogen Production

Thermochemical water splitting processes use high-temperature (500°C – 2,000 °C) to drive a series of chemical reactions that produce hydrogen and oxygen. Actually, thermochemical separation of water occurs in three steps; oxygen production, hydrogen production and recycling of used materials. The main steps are heat and electricity production, thermochemical decomposition of water and purification of produced hydrogen and oxygen. Several catalysts are being investigated in order to achieve decomposition at lower temperatures and the required temperature was reduced to ≈ 1000 ºC for multi-step thermal chemical processes and the total yield was found to be 50% [32].

1.2.3.4. Reformation of Biomass and Wastes

Biomass contributes about 12% of today's world energy supply. Hydrogen can be produced by the pyrolysis or aeration of biomass resources; for instance, woody energy crops, industrial crops, agriculture crops, animal waste, forestry waste and residues and industrial and municipal wastes. A liquid product (bio-fuel) with a wide range of components that can be separated into valuable chemicals and fuels such as hydrogen can be produced by biomass pyrolysis [38].

1.2.3.5. Water Electrolysis

Water splitting studies to produce hydrogen as an energy carrier have been started by the year of 1789 and it is still being investigated by researchers. Although using renewable sources have some advantages, it has also some disadvantages. Amount of energy which is obtained from renewable source are not sufficient for the whole world and it is expensive process compared to energy production from non-renewable

sources. Water splitting is known as the simplest method for the production of hydrogen. Compared with the widely used steam-reformed hydrogen, electrocatalytic production of hydrogen from water splitting is one of the most promising ways for energy conversion. This way has many advantages such as production of highly pure hydrogen, manufacturing capability with small size, transposability, simplicity, environmentally friendly and renewability. Therefore, hydrogen production, which depends on water electrolysis, attracts more attention.

Electrochemical water splitting generally conducted in an electrolysis cell which consists of an electronic conductor, electrodes, and an ionic conductor. electrolyte. When water is electrolyzed, water split into hydrogen and oxygen at the cathode and anode, respectively. Beside its advantages, electrolytic water splitting has also some disadvantages such as high cost and high energy consumption. Products of this reaction are given in Equation (1).

$$2\ H_2O + \text{Energy} \leftrightarrows 2H_2 + O_2 \qquad (1)$$

With an external voltage applied to the electrodes, water molecules dissociate into hydrogen and oxygen. Oxygen is released into the atmosphere whereas the hydrogen can be stored as fuel. According to Faraday's laws, for each one ampere, 0.037 g H_2 and 0.298 g O_2 are released in every one hour. Regardless of the media, water splitting reaction requires thermodynamic potential difference of 1.23 V vs. NHE at 25 ˚C and 1 atm to produce H_2 and O_2. It is noteworthy that thermodynamic potential difference depends on temperature and the overpotential required for the electrolysis decreases with increasing temperature. Nonetheless, higher voltage than the thermodynamic potential value (i.e. 1.23 V vs. NHE at room temperature) is needed to accomplish electrochemical water electrolysis [39]. The excess potential is known as overpotential, η which is used to overcome the intrinsic activation barriers existing such cathodic (η_c) and anodic (η_a) overpotentials together with some other resistances (η_{other}) (i.e. contact resistance and solution resistance). Therefore, operational potential (E_{op}) of water electrolysis can be expressed as given in equation (2):

$$E_{op} = 1.23\ V + \eta_a + \eta_c + \eta_{other} \qquad (2)$$

There are many reasons for overpotential and the most important ones are; activation or charge transfer tension, concentration tension, resistance polarization, reaction overpotential and crystal overpotential. Although, η_{other} can be minimized with proper design of the electrochemical cell, however, highly active hydrogen evolution and oxygen evolution catalysts are needed to minimize η_c and η_a, respectively [40]. Moreover, active electrode area is another significant parameter in detecting overpotential of the reaction because if the active surface area of electrode increases, activation of electrode material also increases [3].

1.3. Electrochemistry of Hydrogen Evolution Reaction (HER) and Oxygen Evolution Reaction (OER)

Water electrolysis consists of two half reaction which are oxygen evolution reaction (OER) and hydrogen evolution reaction (HER). OER is the oxidation part and HER is the reduction part which occurs at the anode and cathode, respectively. Products and the equilibrium half-cell potentials (E°) of hydrogen evolution reaction in acidic and alkaline solution are given in Equation (3) and (4), respectively.

$$2H^+ + 2e^- \rightarrow H_2 \qquad E°= 0.00 \text{ V vs. NHE} \qquad (3)$$

$$2H_2O + 2e^- \rightarrow H_2 + 2OH^- \qquad E°= 0.826 \text{ V vs. NHE} \qquad (4)$$

The HER generally involves three possible reaction steps in acidic medium, while the HER mechanism in alkaline media is still ambiguous. The first one in acidic media is the so-called Volmer step, and the following step may be the Tafel step or the Heyrovsky step depending on reaction mechanism of modified electrode for HER (These steps are explained in experimental part of 2.5.3. (a), clearly).

Oxygen evolution reaction (OER) is more complicated than HER because it contains oxidation of two H_2O molecules with four electrons and then four protons are produced together with O_2 molecule [41]. The equilibrium half-cell potentials (E°) at 1 atm and 25 °C for OER are shown for in alkaline and acidic solution as following Equation (5) and (6), respectively.:

$$4OH^- \rightarrow O_2 + 2H_2O + 4e^- \qquad E° = 0.404 \text{ V vs. NHE} \qquad (5)$$

$$2H_2O \rightarrow O_2 + 4H^+ + 4e^- \qquad E° = 1.230 \text{ V vs. NHE} \qquad (6)$$

As illustrated, transfer of four electrons are required for production of O_2 molecule, and kinetically favorable OER process occurs through multi-step reactions with single-electron transfer at each step. Therefore, energy accumulation at each step slows down the OER kinetics very much and causes large overpotential thus, an electrocatalyst with high activity and stability is desired to overcome the energy barrier [42]. Considerable research efforts have been devoted to find alternative catalysts with better OER activity. Currently, large number of catalysts have been developed, inclusive of noble metal based [43], carbon based (graphene and graphene oxide, CNT etc.) [44], non-noble metals based (Mn, Cu, Ni, and Fe etc.) [45, 46] and so on.

1.4. Catalytic Effect of Modified Electrode

Catalysts are substances that increase the speed of a chemical reaction without being consumed [47] and in electrochemical reaction, modified electrodes are on the role of catalysts. At constant overpotential, if a reaction occurs faster by using one electrode than the other, this electrode is said to be more electrocatalytic than the other. Electrocatalytic activity of electrodes can be compared in terms of overvoltage (ɳ) required to keep the current density, j ($mA.cm^{-2}$) constant. Ideal catalyst needs low overpotential to generate large current densities [3, 42].

Usually, a suitable catalyst is required to decrease the overpotential for electrochemical water splitting reaction and to increase the catalytic activity [48]. It is well known that the most effective catalyst for HER under acidic condition is platinum (Pt), which has near-zero overpotential [49]. It needs very low overpotential to generate large cathodic current densities and it has fastest reaction rate for HER because of the strength of the Pt-H bond [50]. Beside this, using Pt as a catalyst has some disadvantages including its high price and deficiency of Pt element in the Earth's crust [51, 52]. Hence, for HER, developing a cheaper alternative electrocatalysts to platinum is an attractive issue and there are many examples in the literature [53, 54]. However, it is still a big

challenge to develop catalysts with high catalytic activity, reusability, and long life-time for HER under acidic conditions. As an alternative to platinum, ruthenium (Ru) complexes are one of the most favored transition metal due to its high performance, stability and versatility [55] in many types of reactions such as steam-reforming reaction of methane [56], hydrogenation of lactic acid to 1,2-propanediol [57] and CO oxidation [58]. Moreover, in the literature, there are many examples of Ru^0 supported catalysts which were used in hydrogen generation from the hydrolysis of ammonia borane [59, 60]. In fact, there are also some reports utilizing electrochemical activity of Ru and Ce containing catalysts in many types of reactions such as; electrochemical enhancement of catalytic activity of Ru NPs supported on CeO_2 for ethylene oxidation [61], the effect of Ru and ceria on the complete oxidation of methanol and ethanol [62], the effect of cerium adding to RuO_2-IrO_2 mixed nanocatalysts on the electrocatalytic activity of OER [63]. In fact, there are also limited number of reports utilizing Ru nanosheets [43] or Ru nanoparticles [50] for water splitting. It thus will be fundamentally interesting to study the catalytic property of Ru towards water splitting.

In order to decrease overpotential and increase the efficiency, many catalysts are synthesized and used for water splitting. Therefore, much research effort has centered on the preparation of alternative catalysts to Pt/C for water reduction reaction. One approach is to select non-noble metals to make this process cheaper and available in sustainable energy technologies. In this context, non-noble metals are chosen and then different types of support are used to increase efficiency of catalysts. To illustrate, Lukowski et al., designed highly active hydrogen evolution catalysis from metallic WS_2 nanosheets which is synthesized by chemical vapor deposition with facile chemical exfoliation from WS_2 nanostructures [64]. Some structural and chemical changes noted during exfoliation of WS_2 nanosheets, which increased the electrocatalytic activity of electrodes. To evaluate the electrocatalytic HER activity of modified electrode, WS_2 nanosheets was loaded onto rotating disk electrode (RDE) with a fixed mass loading (1.0 ± 0.2 mg.cm^{-2}) by drop casting. The HER performances were measured in 0.5 M H_2SO_4 solution via linear sweep voltammetry (LSV). This electrode needs an overpotential value of 142 mV vs. RHE to reach a current density

(j) of 10 $mA.cm^{-2}$. Tafel slope of the modified electrode was found to be 70 $mV.dec^{-1}$ and these values are compatible to other reported catalysts non-noble metal nanoparticles in literature [65, 66]. Tian et al., also reported the topotactic fabrication of self-supported nanoporous CoP nanowire arrays on carbon cloths (CC) for HER [1] and the HER performances of CoP nanowire (loading: 920 $\mu g.cm^{-2}$) were investigated in 0.5 M H_2SO_4 solution. This electrode shows very low overpotential value as 38 mV, and needs overpotentials of 67, 100 and 204 mV to reach a current density (j) of 10, 20 and 100 $mA.cm^{-2}$, respectively. Tafel slope and exchange current densities of CoP/CC nanowire were found to be 51 $mV.dec^{-1}$ and 0.288 $mA.cm^{-2}$, respectively.

The other most widely used approach is to select noble metals to make water splitting reaction highly active. To illustrate, Mahmood et al., designed an efficient ruthenium-based catalyst for HER which is made of Ru NPs dispersed within a nitrogenated holey two-dimensional carbon structure ($Ru@C_2N$) via polycondensation reaction [50]. By drop casting, $Ru@C_2N$ was loaded onto rotating disk electrode (RDE) with a fixed mass loading ($\approx$ 285 $\mu g.cm^{-2}$) to elucidate the electrocatalytic HER activity of modified electrode in acidic (0.5 M H_2SO_4) and alkaline (1.0 M KOH) medium. For $Ru@C_2N$ catalyst, η = 22 mV vs. RHE overpotential value is needed to reach a current density (j) of 10 $mA.cm^{-2}$. Tafel slope of modified electrode was found 30 $mV.dec^{-1}$ and exchange current density of $Ru@C_2N$ is 1.90 $mA.cm^{-2}$ in acidic medium. Electron transfer resistance (R_{et}) of $Ru@C_2N$ was also investigated by using electrochemical impedance spectroscopy (EIS) and it is found as 43.7 Ω [67]. Stability of $Ru@C_2N$ was also investigated by using cyclic voltammogram and it was found that electroactivity of catalyst does not change after 10,000 CV cycles indicating excellent stability/durability in acidic medium. Durability of the electrode was also tested in alkaline medium and perfect durability of electrode observed like in acidic medium. TOF values were found as 0.67 s^{-1} and 1.95 s^{-1} at overpotentials of 25 and 50 mV, respectively. Furthermore, Zhu et al., also reported a highly active water reduction catalyst with a simple synthesis of an intermetallic Pt_2Si electrode using magnetron sputtering synthesis and electrocatalytic activity of this electrode (mass loading: 100 $\mu g.cm^{-2}$) was also investigated in 0.5 M H_2SO_4 [68]. For Pt_2Si-MS, 78 mV vs. RHE overpotential value is needed to reach current density (j) of 40 $mA.cm^{-2}$. Tafel slope

of the modified electrode found as 30.5 mV.dec^{-1} which indicates that Volmer-Tafel mechanism is predominating for HER. Exchange current density and R_{et} of Pt_2Si were found to be 0.330 mA.cm^{-2} and 1.457 Ω, respectively in 0.5 M H_2SO_4 solution.

Development of efficient electrocatalysts with high activity and low price for water oxidation reaction is also very important for artificial photosynthetic and solar fuel production systems nevertheless, it is still major scientific challenge. Zhu et al., reported a catalyst for water oxidation reaction, Fe–Co_3O_4@Fe–Co–Bi /CC, the OER activity of this catalyst (loading level: 1320 μg.cm^{-2}) was investigated in 0.1 M BK_3O_3 (pH= 9.2) [69]. The TOF values at overpotentials of 400 and 500 mV were found as 0.14 s^{-1} and 0.55 s^{-1}, respectively. Also, this catalyst shows durability for long-term measurement in alkaline solution. Fe–Co_3O_4@Fe–Co–Bi /CC needs overpotential values of 384 mV and 420 mV to reach a current density (j) of 5 mA.cm^{-2} and 10 mA.cm^{-2}, respectively. Tafel slope was determined as 121 mV.dec^{-1}, which is comparable to other reported electrocatalysts [44, 70]. There are many examples of catalyst which works only for HER or OER reaction in the literature. However, there are few examples of bifunctional/dual catalysts and, thus, designing of efficient catalyst for both HER and OER reaction is a very attractive issue [71, 72]. Furthermore, the use of a bifunctional catalyst simplifies the system, decreasing the manufacturing price and so the cost of the resulting hydrogen. Tang et al., designed an efficient and stable dual catalyst for full water splitting is using NiSe nanowire film supported on Nickel foam (NiSe/NF) [73]. The HER and OER activity of NiSe/NF was investigated in alkaline (1.0 M KOH) medium. The Tafel slope for NiSe/NF was found as 64 mV.dec^{-1} for water oxidation reaction. On the other hand, the Tafel slope for NiSe/NF was found as 120 mV.dec^{-1} for water reduction reaction in alkaline medium. Durability of NiSe/NF was also investigated by using chronopotentiometry method for both positive (1.56 V) and negative potentials (-182 mV) and almost no change in the electroactivity of catalyst was noted within 12 hours indicating reasonable durability in alkaline medium. Other examples of efficient catalyst for HER in acidic or alkaline medium are listed in Table 2.

Table 2. Summary of some recently reported representative HER electrocatalysts together with Ru^0/CeO_2 (1.86% wt. Ru) modified gGCE in acidic electrolytes. Data were recorded [a] without and [b] with iR compensation (i: Current, R: Resistance)

Catalyst	Reaction Medium	Loading density ($\mu g.cm^{-2}$)	Tafel Slope ($mV.dec^{-1}$)	j ($mA.cm^{-2}$)	η (mV) at defined j	j_0 ($mA.cm^{-2}$)	Ref.
20% Pt/C	0.5 M H_2SO_4	570	29	10	35	--	74
Ru@C_2N	0.5 M H_2SO_4	285	30	10	22	1.900	50
Ru-MoO_2/GCE (S2) [a]	1.0 M KOH	285	31	10	29	--	74
Pt_2Si	0.5 M H_2SO_4	100	30.5	40	78	0.330	68
Ru^0/CeO_2 [b]	0.5 M H_2SO_4	197	33.41	10 20	41 53	0.540	This Work
$CoSe_2$ on carbon fiber	0.5 M H_2SO_4	2200	40	10 20 100	137 150 181	0.0049	75
Pt-MoS_2	0.5 M H_2SO_4	75	40	10	53	--	67
Ru^0/CeO_2 [a]	0.5 M H_2SO_4	197	41.18	10 20	47 65	0.670	This Work
Mo_2C NPs	0.5 M H_2SO_4	250	41	10	78	0.179	76
Ru-MoO_2/GCE (S2) [a]	0.5 M H_2SO_4	570	44	10	55	--	74
MoP/ Mo_2C@C	0.5 M H_2SO_4	453	45	10	89	0.215	77
Amorphous MoP	0.5 M H_2SO_4	1000	45	10 20	90 105	0.120	78
Ru nanosheet [b]	0.5 M H_2SO_4	~100	46	10 ($mA.mg^{-1}$)	20	-	43
Ru/GLC	0.5 M H_2SO_4	400	46	10 20 50	35 61 125	--	79
Ni_2P	0.5 M H_2SO_4	1000	46	10 20 100	100 130 180	0.033	80

CoP / Ti	0.5 M H_2SO_4	2000	50	20	85	0.140	65
WS_2NDs	0.5 M H_2SO_4	16.3	51	--	--	0.110	2
CoP nanowire	0.5 M H_2SO_4	920	51	10 20	67 100	0.288	1
P-WN/rGO	0.5 M H_2SO_4	337	54	10	85	0.350	81
MoN-NC	0.5 M H_2SO_4	145	54	10	62	0.778	82
CoS|P/CNT	0.5 M H_2SO_4	1600	55	10 20 100	48 65 109	1.140	34
Mo_2C/CNT	0.1 M $HClO_4$	2000	55.2	10	152	0.014	83
CoPS NP|S	0.5 M H_2SO_4	360	56	10	48	0.984	84
WS_2/RGO	0.5 M H_2SO_4	400	58	10 20	265 292	--	66
Mo_2C@NC	pH= 0	--	60	10	60	0.960	35
Co-NRCNTs	0.5 M H_2SO_4	280	69	1.0 10	140 260	0.01	85
N-WS_2-H_2	0.5 M H_2SO_4	320	70	100	197	0.174	48
WS_2 nanosheets	0.5 M H_2SO_4	1000	70	10	142	--	64
Long Ru-TiNT	1.0 M $HClO_4$	--	70	50 100	170 190	0.180	86
C/CoSnZn-Pd	1.0 M KOH	--	70	100	124	1.900	87
Commercial Ru/C [b]	0.5 M H_2SO_4	--	72	10	69	--	79
Ru/SiNWs	0.5 M H_2SO_4	257	81	10 30	200 258	--	88
NiSe/NF	1.0 M KOH	2800	120	10	96	--	73
β-Mo_2C	0.1 M $HClO_4$	280	120	1.0	200	0.017	89
IrNi NCs	0.5 M H_2SO_4	12.5	--	20	21	--	90
NiFe LDH@NF	1.0 M NaOH	--	--	10	210	--	91
Hydrous RuO_2/Ni foam	1.0 M KOH	520	--	10	60	--	92

1.5. Aim of This Study

Compared with the widely used steam-reformed hydrogen, electrocatalytic production of hydrogen from water electrolysis is one of the most promising ways for energy conversion. The main obstacle in the electrolytic hydrogen production from water is the high overpotential of HER and much effort have been devoted to the development of highly efficient and stable electrocatalysts for reducing the overpotential in electrolytic water splitting. Therefore, we have investigated the electrocatalytic response of GC electrodes modified with ruthenium(0) nanoparticles supported on different reducible oxides such as ceria (CeO_2), titania (TiO_2), hafnia (HfO_2) and zirconia (ZrO_2) in water splitting. Our main aim was not only to investigate the effect of different supporting materials but also to investigate the amount of ruthenium(0) nanoparticles on the overpotential for HER and several electroanalytical techniques (i.e linear sweep voltammetry, cyclic voltammetry, constant potential electrolysis and electrochemical impedance spectroscopy) were used for this purpose.

CHAPTER 2

EXPERIMENTAL

2.1. Chemicals

Nanoceria (CeO_2, particle size ≈ 25 nm), nanotitania (TiO_2, particle size ≈ 25 nm), nanozirconia (ZrO_2, particle size ≈ 100 nm), hafnia(IV) oxide (HfO_2, powder) and nafion perfluorinated resin solution (5% wt. in lower aliphatic alcohols and water, contains 15-20% water) were purchased from Aldrich. Ruthenium(III) chloride hydrate ($RuCl_3 \cdot 3H_2O$) and sodium borohydride ($NaBH_4$, 98%) were purchased from Merck. Deionized water was distilled by Milli-Q water purification system. All glassware and Teflon-coated magnetic stir bars were cleaned with acetone, followed by rinsing with distilled water before drying in an oven at 110 °C.

2.2. Preparation of Ru^0/MO_2 (M= Ti, Zr, Hf and Ce) catalysts

Desired amount of metal oxide was added to a solution $RuCl_3 \cdot 3H_2O$ in 100 mL H_2O in a 250 mL round bottom flask. This slurry was stirred at room temperature for 24 hours and then, $NaBH_4$ solution (a required amount of sodium borohydride was weighed by keeping $NaBH_4$/Ru ratio as 3 for all tests and dissolved in 10 mL H_2O) was added dropwise. After about 1 hour stirring, Ru^0/MO_2 were formed and the samples were isolated by centrifugation and washed several times with 100 mL of water. The remnant was dried under vacuum at 60 °C for 12 hours. For comparison Ru^0/TiO_2, Ru^0/ZrO_2, Ru^0/HfO_2, and Ru^0/CeO_2 at different loading levels were prepared by using $RuCl_3 \cdot 3H_2O$ in the amount required for the desired ruthenium loading by following the same procedure as described above. The ruthenium contents

of all the samples were determined by ICP-OES (see Table 3 for the amount of used materials).

Table 3. The amount of materials for the preparation of the Ru^0/MO_2 (M = Ti, Zr, Hf, Ce) catalysts.

Catalyts	Desired Loading (wt %)	Metal oxide (mg)	$RuCl_3.3H_2O$ (mg)	H_2O (mL)	$NaBH_4$ (mg) 3 eqv.
Ru^0/TiO_2	2	600	32.75	100	14.27
Ru^0/ZrO_2	2	600	32.75	100	14.27
Ru^0/HfO_2	2	600	32.75	100	14.27
Ru^0/CeO_2	1	1000	26.567	100	11.57
Ru^0/CeO_2	2	600	32.75	100	14.27
Ru^0/CeO_2	3	500	42.08	100	18.33
Ru^0/CeO_2	4	800	92.38	100	40.26
Ru^0/CeO_2	5	500	74.40	100	32.42
Ru^0/CeO_2	6	500	91.90	100	40.00

2.3. Characterization of Metal Nanoparticles

The ruthenium content of Ru^0/MO_2 (M = Ti, Zr, Hf, Ce) samples was determined by the Inductively coupled plasma optical emission spectroscopy (ICP-OES, Leeman-Direct Reading Echelle) after each sample was completely dissolved in the mixture of HNO_3/HCl (1/3 ratio).

Transmission electron microscopy (TEM) was performed on a JEM-2100F (JEOL) microscope operating at 200 kV. A small amount of powder sample was placed on the holey carbon grid of the transmission electron microscope. Samples were examined at magnification between 100 and 400 K. The elemental analysis was performed by using

an energy dispersive X-ray (EDX) analyzer (KEVEX Delta series) mounted on the Hitachi S-800.

The X-ray diffraction (XRD) pattern was performed on a MAC Science MXP 3TZ diffractometer using monochromatic Cu-Kα radiation with a wavelength of 1.5406 Å, the X-ray tube working at 40 kV, 55 mA.

The X-ray photoelectron spectroscopy (XPS) analysis was performed on a Physical Electronics 5800 spectrometer equipped with a hemispherical analyzer and using monochromatic Al Kα radiation (1486.6 eV, the X-ray tube working at 15 kV, 350W and pass energy of 23.5 keV).

2.4. Preparation of Electrode Solution

In a typical electrochemical measurement, desired amount of catalyst (see the Table 4 for desired amount of catalyst with respect to the loading level and metal oxide) and 20 μL Nafion solution were dispersed in water (1.5 mL) /isopropanol (1.0 mL) solution and sonicated for 60 min to form homogeneous mixture. Then, a 5 μL aliquot of this mixture containing ≈13.8 μg catalyst, which was kept constant for all electrochemical measurements, was dropped onto a polished glassy carbon electrode with 3 mm in diameter. After loading the catalyst, the electrode was kept in an oven at 100 ºC for 12 hours [43].

Table 4. Desired amount of the catalyst with respect to loading level and metal oxide added to the nafion/isopropanol/water mixture to maintain the same amount of ruthenium content on the glassy carbon electrode. (Metal contents were determined by ICP-OES)

Catalyst	Loading Level (%)-Theoretical	Loading Level (%)-Experimental	Desired Amount (mg)
Ru^0/TiO_2	2	1.20	579.65
Ru^0/ZrO_2	2	1.41	493.33
Ru^0/HfO_2	2	2.00	347.80
Ru^0/CeO_2	1	0.92	756.08
Ru^0/CeO_2	2	1.86	373.76
Ru^0/CeO_2	3	2.98	233.42
Ru^0/CeO_2	4	3.95	176.10
Ru^0/CeO_2	5	4.90	141.96
Ru^0/CeO_2	6	5.96	116.71

2.5. Characterization of Modified GC Electrodes

2.5.1. Electrochemical Cell

Typically, electrochemical cell consists of three electrodes, which are GC working electrode with 3.00 mm in diameter, Pt wire counter electrode and Ag/AgCl reference electrode. All GCEs were cleaned by using alumina polishing suspension before performing the electrochemical measurements.

2.5.2. Electrochemical Measurements

Electrochemical measurements were performed by using a Gamry PCI4/300 potentiostat–galvanostat at room temperature. Electrochemical behaviors of the modified electrodes were investigated in 0.5 M H_2SO_4 and 0.5 M KOH solutions purged with pure N_2 and polarization curves were recorded at a scan rate of 5 $mV.s^{-1}$. The potentials obtained from linear sweep voltammetry (LSV) experiments were calibrated with respect to reversible hydrogen electrode (RHE) by adding a value of (0.197 + 0.059 pH) V [40]. The electrochemical impedance spectroscopy (EIS) measurements were conducted at various potentials with amplitude of 10 mV and in the frequency range of 0.01–100000 Hz. The stability of modified electrodes was investigated both by recording the cyclic voltammograms (CV) in the same electrolyte solution in a potential range of -0.50 to +0.60 V versus Ag/AgCl at a voltage scan rate of 100 $mV.s^{-1}$ or via controlled potential electrolysis at an applied constant potential of 0.350 V vs. Ag/AgCl.

2.5.3. Experimental Methods for Characterizing the Electrochemical Activity of Modified GC Electrode

The important parameters that determine the activity of modified GC electrodes towards water splitting include Tafel slope, exchange current density, stability, turnover frequency (TOF), as well as electron transfer resistance.

2.5.3.1. Tafel Plot

Tafel analysis is often used to understand the reaction mechanism and kinetics and to compare the catalytic activity of different types of electrodes. HER generally involves three possible reaction steps in acidic media. First step of HER in acidic media is called as Volmer step, $H^+ + e^- \rightarrow H_{ad}$ (electrochemical hydrogen adsorption) which is usually considered as fastest step. In this step, adsorbed hydrogen atom (H_{ad}) forms on the electrode surface as a result of reaction between an electron and proton. After this step, hydrogen evolution reaction may continue with lower hydrogen evolution

process; the Heyrovsky step (electrochemical desorption) or the Tafel step (chemical desorption) or both [93].

Heyrovsky step: $H_{ad} + H^+ + e^- \rightarrow H_2$

Tafel step: $H_{ad} + H_{ad} \rightarrow H_2$

Moreover, the rate determining step in the HER mechanism could be Volmer - Tafel, or Volmer – Heyrovsky. Tafel slopes in the region of 30 $mV.dec^{-1}$ have been observed for the HER on the noble metals, they have been variously attributed to the Volmer-Tafel mechanism. If (H) is the only adsorbed species, the theory predicts that Tafel slope for the Volmer- Heyrovsky mechanism has its lowest value of 40 $mV.dec^{-1}$ [94]. Figure 6 shows the mechanism of Volmer - Tafel and Volmer - Heyrovsky (blue arrows indicate Volmer step, red arrow shows Tafel step and violet arrow indicates Heyrovsky step). The Tafel equation (shown in Equation 7) is used to define the rate determining step by examining the steady state current density on a variety of overpotential.

$$\eta = a + b\log j \qquad (7)$$

where $\boldsymbol{\eta}$ is overpotential value, b represents the Tafel slope, j is the current density. With a low Tafel slope, HER rate of a catalyst will increase rapidly with increasing overpotential.

Whereas exchange current density, $\mathbf{j_0}$, which is obtained when η is assumed to be zero, describes the intrinsic catalytic activity of the electrode material under equilibrium conditions. It represents the rates of both oxidation and reduction for an electrode at equilibrium. Larger the exchange current density leads to faster the reaction, and vice versa. To conclude, for an ideal catalyst for HER, high j_0 and a small Tafel slope (b) is desirable.

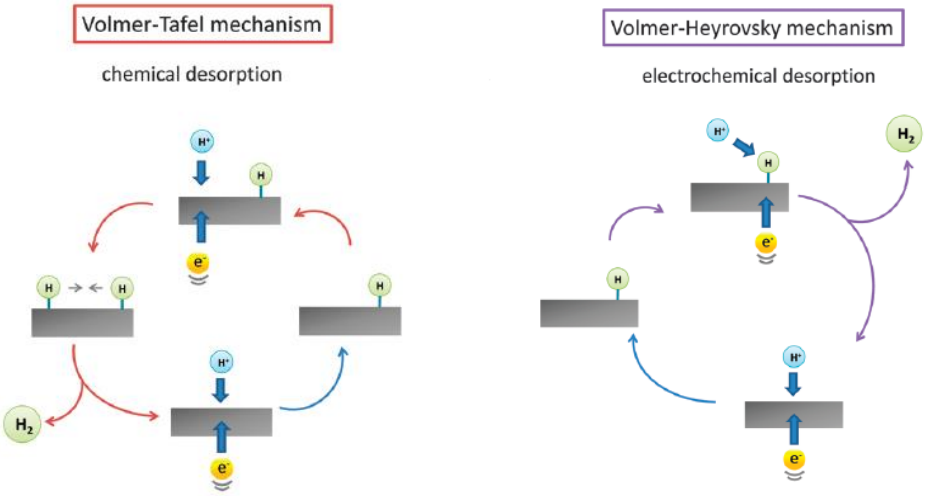

Figure 6. Different mechanisms of hydrogen evolution on the surface of an electrode in acidic solution [4].

2.5.3.2. Stability

It is important to state that the one of the best parameter to characterize an electrocatalyst is its stability. Two methods are commonly used to determine the stability of any catalysts. In the first method, the electrode containing the electrocatalyst is subjected to repetitive cycling between certain potential ranges via cyclic voltammetry. Then the onset potential, over potential and current densities were determined from polarization curves by recording LSV, after potential cycling. The other method is employing constant potential to electrode for a long time and variation of current density with time was monitored a small change or no change indicates high stability of the modified electrode [3].

2.5.3.3. Faradaic Efficiency

Faradic efficiency defines the efficiency of electrons to participate in the desired reaction in an electrochemical system. For the electrochemical H_2 and O_2 evolution reaction, Faradaic efficiency is described as the ratio of the amount of experimentally determined H_2 and O_2 to the theoretical amount of H_2 and O_2, which can be calculated

from the current density based on a 100% Faradaic yield [3]. HER and OER activity of a catalyst is determined by measuring the amount of hydrogen and oxygen released during water splitting by using modified electrodes in a Hoffman electrolysis apparatus (see Figure 7).

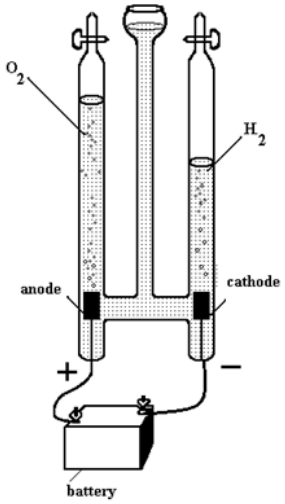

Figure 7. Hoffman electrolysis apparatus with a power supply.

2.5.3.4. Turnover Frequency (TOF)

A catalytic cycle is a co-rotating wheel of many chemical steps in a common "speed". In a reaction that is first-order in the catalyst and in steady state, this speed is explained by the turnover frequency (TOF) of the cycle. With the help of catalyst number of reactant converting to a desired product per catalytic site per unit of time is defined as TOF, and thus it is crucial parameter to interrogate to efficiency of any catalyst. TOF value can be evaluated using the Equation (8) given below [95].

$$TOF = \frac{j}{2nF} \qquad (8)$$

where j is current density for different samples during LSV measurement in 0.5 M H_2SO_4, n represents number of active sites which can be calculated by using n= Q/ 2F

formula, the integrated charge, Q over the whole potential range was divided by two [96]. Then, the value was divided by the Faraday constant (F= 96485 $C.mol^{-1}$) to get the number of active sites for different samples.

2.5.3.5. Electron Transfer Resistance (R_{et})

An alternative current (AC) is used to signal process for EIS measurements. According to the characteristic of AC, electrical wave shaped frequency is generated in a wave form potential (E) and current (I). The basic of the spectrum is "frequency" and different frequencies form a spectrum. Therefore, impedance is calculated by using this spectrum data.

Impedance measurement diagram of EIS in the form of Nyquist plot which is constructed in 2-dimension (2D) on X and Y axis. Real part of impedance (Z_{re}) is shown on the X-axis of Nyquist plot, and X-axis represents W, R_{et} and R_s values in the unit of Ohm whereas, imaginary part of impedance ($-Z_{im}$) is shown on Y-axis of the Nyquist plot [97].

Electron transfer resistance is the resistance against the process of electron transfer from one phase (e.g. electrode) to another (e.g. electrolyte). The high polarization resistance causes the electron transfer kinetics to slow down and the R_{et} to be high [87]. Furthermore, R_{et} values can also be used to evaluate the exchange current densities (j_o) at each overpotential value (η) by using Equation (9).

$$j_0 = \frac{RT}{nFR_{et}} \qquad (9)$$

In Equation (9), R represents the gas constant (R= 8.314 $J.K^{-1}.mol^{-1}$), T is the temperature at which the experiment is conducted, F is the Faraday constant (F = 96485 $C.mol^{-1}$), n is the number of transferred electrons and R_{et} is the electron transfer resistance in ohm (Ω) of the modified GC electrode.

CHAPTER 3

RESULTS AND DISCUSSIONS

3.1.Preparation and Characterization of Ruthenium(0) Nanoparticles Stabilized Ceria (CeO_2)

Nanoceria supported Ru(0) nanoparticles (Ru^0/CeO_2) were prepared by impregnation of Ru(III) ions on the surface of ceria followed by their reduction with $NaBH_4$ at room temperature. Ru^0/CeO_2 was isolated from the reaction solution by centrifugation and characterized by ICP-OES, XRD and TEM and EDX. Powder XRD pattern of Ru^0/CeO_2 (1.86% wt. Ru) in Figure 8b exhibits peaks at 28.5º, 33.07º, 47.08º, 56.33º and 59.08º assigned to the (111), (200), (220), (311) and (222) reflections of ceria, respectively (JPDS = 43-1002). The comparison of the XRD patterns (Figure 8) clearly shows that there is no noticeable alteration in the framework lattice or loss in the crystallinity of the ceria after the ruthenium loading. Note that there is no observable peak attributable to ruthenium nanoparicles in Figure 8b, most likely as a result of low ruthenium loading on ceria.

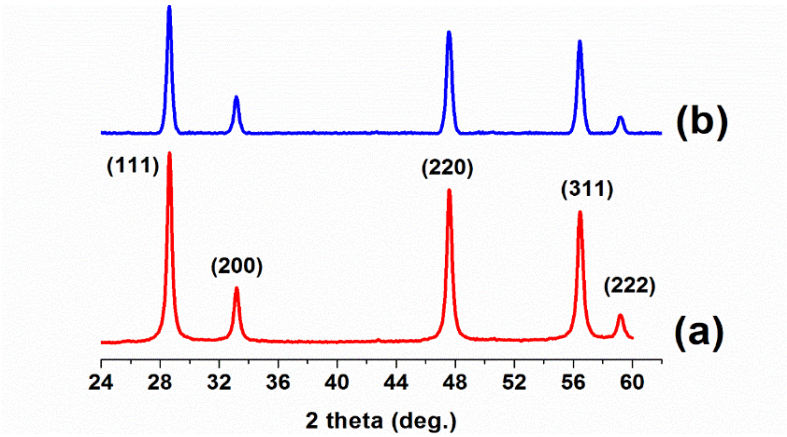

Figure 8. Powder XRD pattern of **(a)** CeO_2 and **(b)** Ru^0/CeO_2 (1.86% wt. Ru).

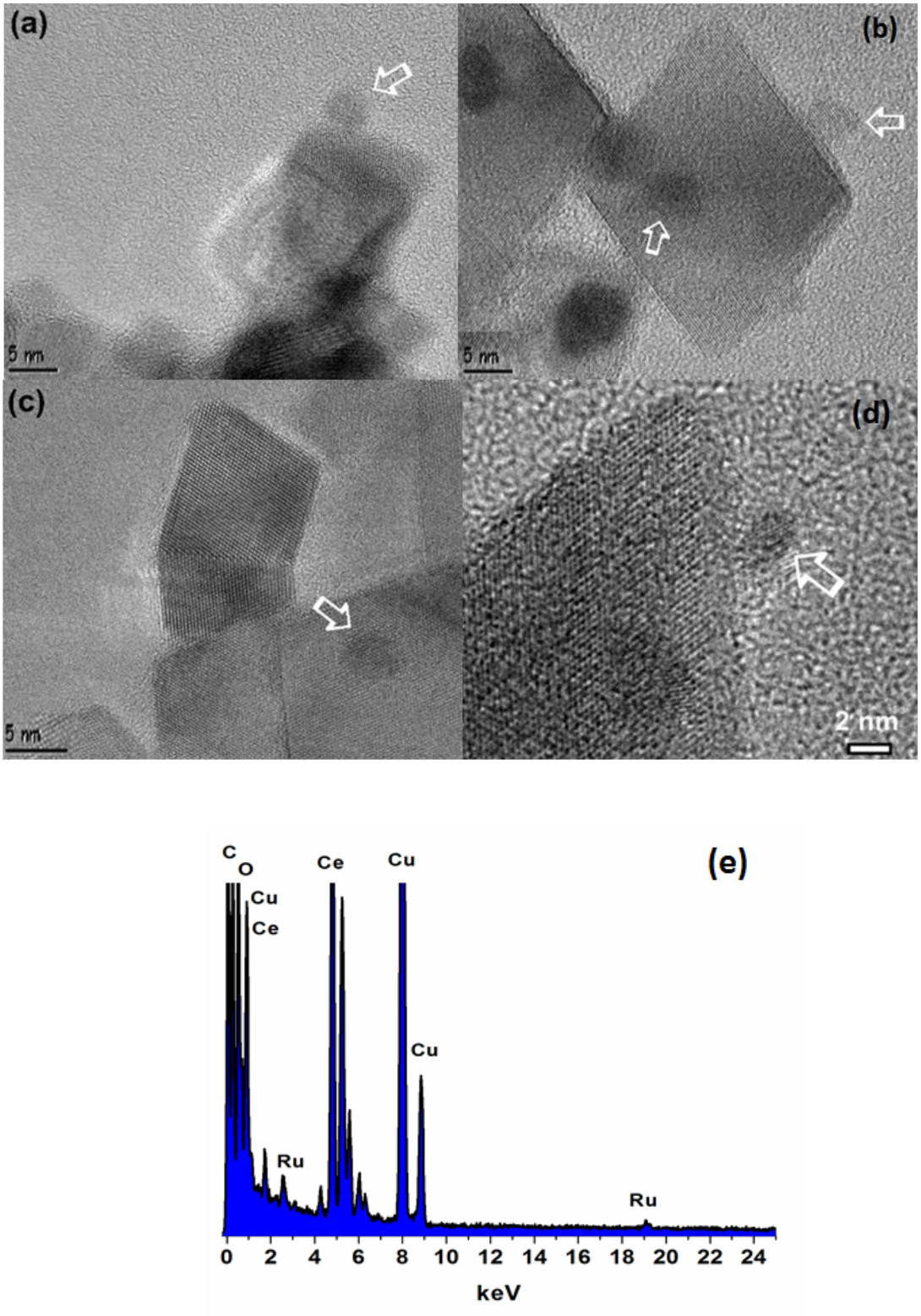

Figure 9. TEM images of Ru^0/CeO_2 (1.86% wt. Ru) at different magnifications **(a–d)** and the corresponding TEM-EDX spectrum **(e)**.

The size of ruthenium nanoparticles on the surface of ceria was investigated by high resolution TEM (Figure 9a–d) showing the dispersion of ruthenium nanoparticles with particle size in the range 2.5–6.0 nm on the surface of ceria nanopowders. Composition of a catalyst was investigated roughly by EDX spectrum (Figure 9e) which reveals that the existance of low loading Ru NPs on the surface of ceria.

High resolution TEM was also used to investigate the size and morhology of ruthenium nanoparticles on the surface of TiO_2, ZrO_2, HfO_2 in Figure A.1, A.2 and A.3, respectively.

In addition, XPS can be used to investigate elements and their distribution on surface of metal nanoparticles stabilized on a support or present in powder form; futhermore, chemical and electronic state are investigated. The survey-scan XPS spectrum of Ru^0/CeO_2 with a ruthenium loading of 1.86% wt in Figure B.1 (a) shows that ruthenium is the only element detected in addition to the ceria framework elements (Ce, O) in agreement with the TEM-EDX result. The high resolution X-ray photoelectron spectrum of a Ru^0/CeO_2 sample given in Figure B.1 (b) shows a prominent band at 279.9 eV which can be readily assigned to Ru(0) $3d_{5/2}$ in the nanoparticles by comparing with the value of ruthenium metal at 280 eV [98]. It is noteworthy that the Ru(0) $3d_{3/2}$ peak at 284.2eV overlaps with the adventitious C 1s peak at 284.0 eV. Because of this overlap, only the peak at 279.9 eV can be assigned to Ru(0) $3d_{5/2}$ with certainty. The higher energy peaks might be of carbon or ruthenium. For comparison, Ce 3d high resolution XPS spectra of CeO_2 and Ru^0/CeO_2 are also given in Figure B.2. Although a slight change is seen in intensity of the Ce 3d bands of Ru^0/CeO_2 compared to those of CeO_2 there is no indication of a noticeable change in the oxidation state of cerium after ruthenium loading.

3.2.Comparison of Electrocatalytic Activity of Ru^0/MO_2 (M= Ti, Zr, Hf, Ce) on GC and Bare GCE in 0.5 M H_2SO_4 for HER

Ru^0/MO_2 nanocomposites were prepared by reduction of ruthenium(III) chloride on different types of metal oxides, which were TiO_2, ZrO_2, HfO_2 and CeO_2 in order to understand the effect of metal oxide support on the electrocatalytic effect of Ru(0) nanoparticles. For this porpose, Ru^0/MO_2 (M= Ti, Zr, Hf, Ce) was loaded onto GC electrode (d = 3.00 mm) with a fixed mass loading (≈ 0.197 $mg.cm^{-2}$) by drop casting. The HER performances were measured in 0.5 M H_2SO_4 solution via linear sweep voltammetry (LSV). Polarization curves obtained utilizing Ru^0/MO_2 modified electrodes are depicted in Figure 10a together with polarization curve for bare GCE for comparison sake. As seen from Figure 10a, onset potentials for the modified electrodes show some differences depending on the type of metal oxide support. The overpotentials for various current densities were also tabulated without IR correction in Table 5. An inspection of Table 5 reveals that Ru^0/CeO_2 modified GCE has the lowest onset potential (33 mV) value and Ru^0/HfO_2-GCE has the highest onset potential (51 mV) value among the four Ru^0/MO_2 modified GC electrodes.

The overpotential values (η) of the Ru^0/MO_2 modified GC electrodes were obtained from polarization curves to derive certain current densities, and the results were given in Table 5 for comparison. Among the catalysts modified GCEs given in Table 5, Ru^0/CeO_2 (1.86% wt. Ru) on GCE requires the lowest overpotential value to reach a current density (j) of 10 $mA.cm^{-2}$ (η = 47 mV) and 20 $mA.cm^{-2}$ (η = 65 mV). On the other hand, Ru^0/TiO_2, Ru^0/ZrO_2 and Ru^0/HfO_2 modified GC electrodes produce cathodic current density (j) of 20 $mA.cm^{-2}$ at η = 75 mV, η = 85 mV, η = 101 mV, respectively. These results indicate that Ru^0/CeO_2 on GCE seems to be better than Ru^0/TiO_2, Ru^0/ZrO_2 and Ru^0/HfO_2 modified GC electrodes for HER. These overpotentials compare favorably well to the behavior of other non-Pt and Pt dependent electrocatalysts in acidic aqueous solutions for HER. For instance, the overpotential at 20 $mA.cm^{-2}$ was found to be 150 mV for $CoSe_2$ [75] and 105 mV for amorphous MoP [78], and the overpotential at 10 $mA.cm^{-2}$ was found to be 53 mV for

Pt-MoS_2 [67] and 55 mV for Ru-MoO_2/GCE [74] (All data are given with respect to the RHE).

Table 5. The onset potentials and over potentials determined at various current densities for the Ru^0/MO_2 (M= Ti, Zr, Hf, Ce) on GC electrodes in 0.5 M H_2SO_4.

Ru^0/MO_2 - GCE	**Onset (mV vs. RHE)**	**η (mV) at 5 $mA.cm^{-2}$**	**η (mV) at 10 $mA.cm^{-2}$**	**η (mV) at 15 $mA.cm^{-2}$**	**η (mV) at 20 $mA.cm^{-2}$**	**η (mV) at 25 $mA.cm^{-2}$**
Ru^0/TiO_2 (1.20% wt. Ru)	40	45	59	67	75	85
Ru^0/ZrO_2 (1.41% wt. Ru)	41	44	61	74	85	97
Ru^0/HfO_2 (2.00% wt. Ru)	51	55	73	88	101	114
Ru^0/CeO_2 (1.86% wt. Ru)	33	37	47	55	65	72

Tafel slopes and exchange current densities were also evaluated from linear sweep voltammograms to inspect similarities or differences between different metal oxide supports and, the results are given in Figure 10b and 10c, respectively. As seen from Figure 10b Ru^0/CeO_2 (41 $mV.dec^{-1}$) modified GC electrode has relatively lower Tafel slopes as compared to Ru^0/TiO_2 (54 $mV.dec^{-1}$), Ru^0/ZrO_2 (49 $mV.dec^{-1}$) and Ru^0/HfO_2 (60 $mV.dec^{-1}$) modified GC electrodes. These values indicate that electrochemical desorption process is the rate-limiting step and it is explained in terms of Volmer−Heyrovsky mechanism [34]. Experimentally obtained Tafel slopes for Ru^0/MO_2-GC electrodes are comparable to or even better than those of recently reported catalyst for HER reaction inclusive of CoP nanoparticles on a Ti support (50

$mV.dec^{-1}$) [65], MoN-NC (54 $mV.dec^{-1}$) [82], Co|SP/CNT (55 $mV.dec^{-1}$) [84], commercial Ru/C (72 $mV.dec^{-1}$) and Ru/GLC (46 $mV.dec^{-1}$) [79] in 0.5 M H_2SO_4.

It is known that an ideal catalyst for HER reaction should have low Tafel slope and high exchange current density. Inspection of Figure 10c reveals that the activity of the electrodes for HER increases in the order of Ru^0/TiO_2 (0.71 $mA.cm^{-2}$) > Ru^0/CeO_2 (0.67 $mA.cm^{-2}$) > Ru^0/ZrO_2 (0.62 $mA.cm^{-2}$) > Ru^0/HfO_2 (0.61 $mA.cm^{-2}$). These results, obtained from LSV measurements, indicate that Ru^0/CeO_2 modified GC electrode shows the highest catalytic activity for HER because it has one of the highest exchange current density and lowest Tafel slope among the all modified GCEs. The exchange current densities of Ru^0/CeO_2 (1.86% wt. Ru) catalyst is higher than most of the reported catalysts given in Table 2 in 0.5 M H_2SO_4 such as CoP nanoparticles on a Ti support (0.140 $mA.cm^{-2}$) [65], amorphous MoP (0.12 $mA.cm^{-2}$) [78] and MoN-NC (0.778 $mA.cm^{-2}$) [82]. Although the mechanism of the promoting effect of cerium oxides has not been well understood yet, the high catalytic activity of ceria based catalyst has been attributed to the formation of cerium (III) defects [99] which can readily be formed because of the favorable large positive standard reduction potential of $Ce^{4+} \rightarrow Ce^{3+}$ (1.76 V in acidic solution [100]).

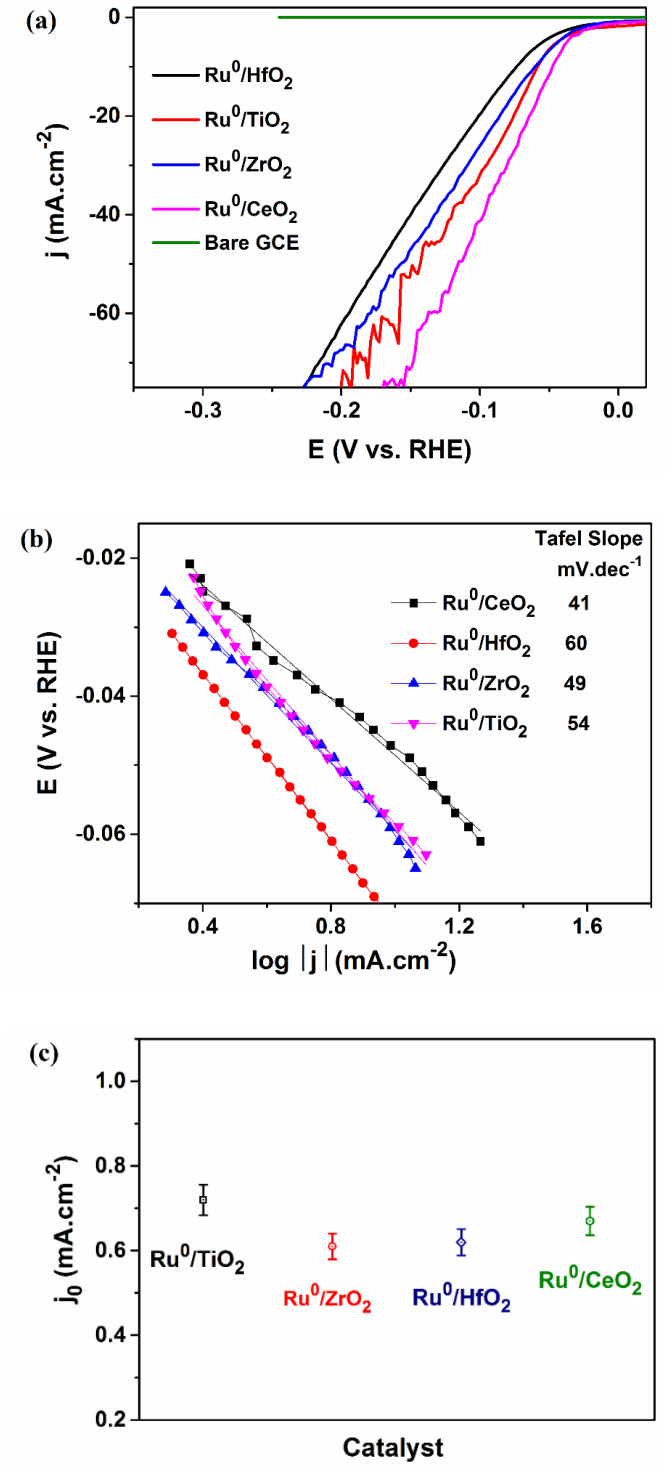

Figure 10. (a) Polarization curves of bare GCE and the Ru^0/MO_2 (M= Ti, Zr, Hf, Ce) samples on GC electrodes in 0.5 M H_2SO_4 at a scan rate of 5 $mV.s^{-1}$, **(b)** The corresponding Tafel plots obtained from polarization curves for HER, **(c)** The corresponding exchange current density of each electrocatalysts for HER.

Since the turnover frequency (TOF) number is a measure of the catalytic activity of the modified electrodes, the TOF values of Ru^0/MO_2 (M= Ti, Zr, Hf, Ce) catalyst was calculated by recording CV of Ru^0/MO_2 modified GCEs in 1.0 M phosphate buffer saline (PBS) solution (pH= 7.4) in the potential range of -0.5 to + 0.6 V vs. Ag/AgCl at a scan rate of 50 $mV.s^{-1}$. The TOF value for the Pt electrode at 0.0 V was found to be 0.80 s^{-1}. To obtain the same TOF value for the modified electrodes, overpotentials of 45, 39, 50 and 28 mV are required for Ru^0/MO_2 (M= Ti, Zr, Hf and Ce, respectively). It is remarkable that Ru^0/CeO_2 (1.86% wt Ru) modified GCE needs lowest overpotential to reach a TOF value of 0.8 s^{-1}.

Table 6. The overpotentials determined to reach the same TOF value, 0.8 s^{-1} for Ru^0/MO_2 (M= Ti, Zr, Hf, Ce) modified GC electrodes together with Pt.

Catalyst	**η (mV vs. RHE)**	**TOF, s^{-1}**
Ru^0/CeO_2 (1.86% wt. Ru)	28.30	0.80
Ru^0/HfO_2 (2.00% wt. Ru)	49.40	0.80
Ru^0/ZrO_2 (1.41% wt. Ru)	38.72	0.80
Ru^0/TiO_2 (1.20% wt. Ru)	44.90	0.80
Pt	0.00	0.80

Electrochemical impedance spectroscopy (EIS) analysis was performed at various overpotentials to determine the catalytic activity of modified electrodes for hydrogen evolution reaction in 0.5 M H_2SO_4. The representative Nyquist plots for Ru^0/CeO_2 (1.86% wt. Ru), Ru^0/TiO_2 (1.20% wt. Ru) and Ru^0/ZrO_2 (1.41% wt. Ru) modified GC electrodes at different overpotentials are given in the Figure 11a and 11b (for Ru^0/CeO_2

on GCE), Figure 12a and 12b (for Ru^0/TiO_2 on GCE) and Figure 13 (for Ru^0/ZrO_2 on GCE). Generally, Nyquist plots obtained at various potentials versus Ag/AgCl for Ru^0/CeO_2, for Ru^0/TiO_2 and for Ru^0/ZrO_2 modified electrodes consist of a small semicircle in the high frequency region due to porous surface of modified electrodes and a larger semicircle in the low frequency region due to electron transfer reaction. These data were modeled by the electrical equivalent circuit as shown in the Figure 14. In this equivalent circuit, R_1 and CPE_1 correspond to high-frequency loop, R_2 and the CPE_2 is related to low-frequency loop and R_s represents the solution resistance. The single loop in the Nyquist curves expresses the electron transfer resistance and diffuse layer resistance and the diameter of the semicircles decreases with the increasing specific overpotentials indicating the decrease in electron transfer resistance, R_{et}.

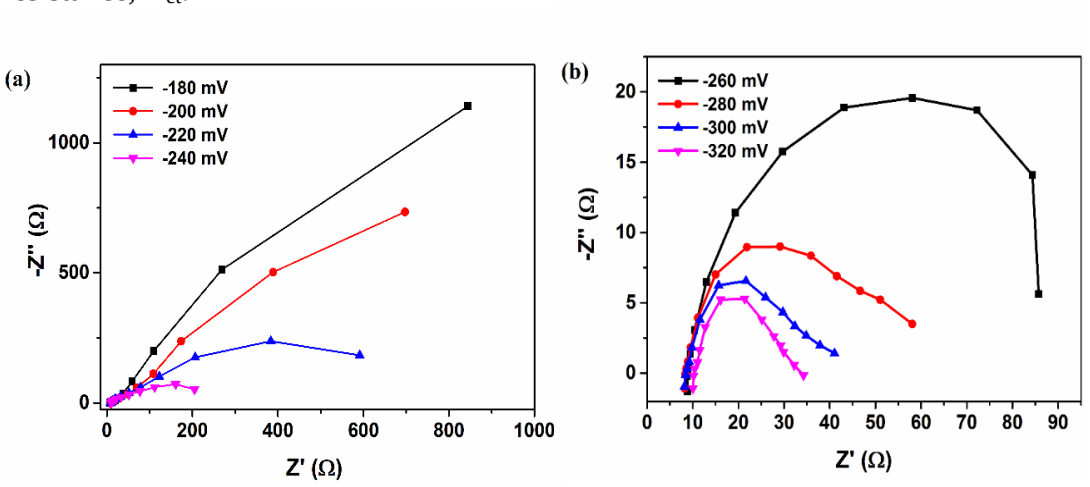

Figure 11. The Nyquist plots for Ru^0/CeO_2 (1.86% wt. Ru) modified GC electrode at different overpotentials vs. Ag/AgCl **(a)** before onset potential **(b)** after onset potential in 0.5 M H_2SO_4.

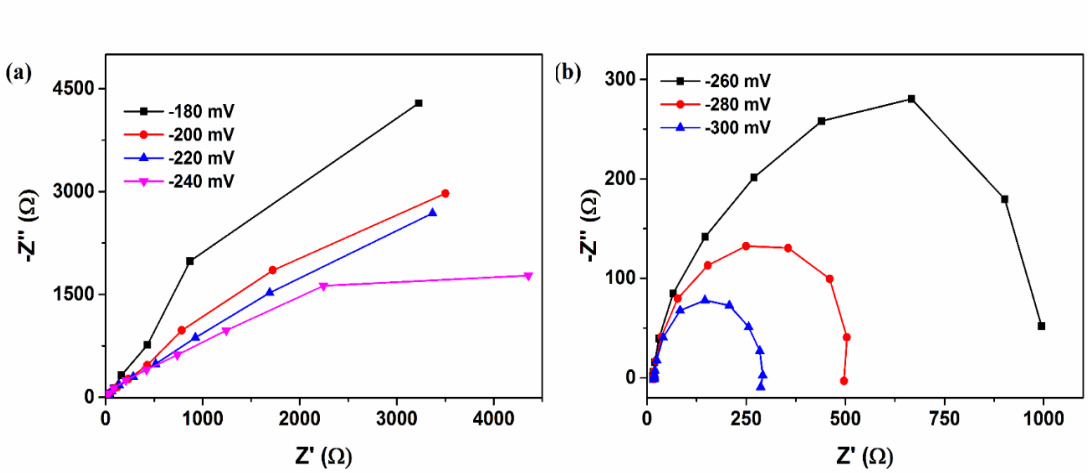

Figure 12. The Nyquist plots for Ru^0/TiO_2 (1.20% wt. Ru) modified GC electrode at different overpotentials vs. Ag/AgCl **(a)** before onset potential **(b)** after onset potential in 0.5 M H_2SO_4.

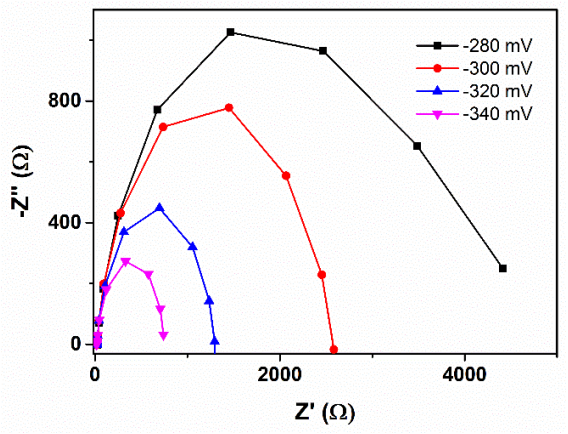

Figure 13. The Nyquist plots for Ru^0/ZrO_2 (1.41% wt. Ru) modified GC electrode at different overpotentials vs. Ag/AgCl after onset potential in 0.5 M H_2SO_4.

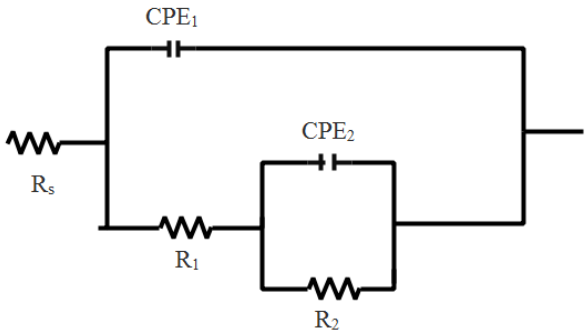

Figure 14. The two time constant serial (CPE-R) model.

It is noteworthy that the Tafel slope value (48 mV.dec^{-1}) obtained from the EIS data by plotting log (1/ R_{et}) versus overpotential (Figure 15) was found to be very close to the one obtained from the LSV (41 mV.dec^{-1}) for Ru^0/CeO_2 modified GCE. In the case of Ru^0/TiO_2 on GCE the Tafel slope value obtained from the EIS data (62 mV.dec^{-1}) as shown in Figure 16 was also found to be very close to the one obtained from the LSV (54 mV.dec^{-1}).

Furthermore, R_{et} values were also used to evaluate the exchange current densities (j_o) at each overpotential value (η) by using Equation 9. As expected, there is an increase in the exchange current densities with the increase in the overpotential values (See Table 7 for Ru^0/CeO_2 modified GCE and Table 8 for Ru^0/TiO_2 modified GCE).

Table 7. Exchange current densities (j_0) and electron transfer resistances (R_{et}) of Ru^0/CeO_2 (1.86% wt. Ru) modified GC electrode with respect to overpotential.

η (mV vs. Ag/AgCl)	**R_{et} (Ω)**	**j_0 (mA.cm^{-2})**
180	6006	0.061
200	4835	0.076
220	812	0.45
240	793	0.46
260	127	2.90
280	29	12.47
300	31	11.77
320	23	15.88

Table 8. Exchange current densities (j_0) and electron transfer resistances (R_{et}) of Ru^0/TiO_2 (1.20% wt. Ru) modified GC electrode with respect to overpotential.

η (mV vs. Ag/AgCl)	**R_{et} (Ω)**	**j_0 (mA.cm^{-2})**
180	14598	0.0251
200	9153	0.0401
220	8764	0.0419
240	1928	0.190
260	1044	0.351
280	518	0.707
300	296	1.240

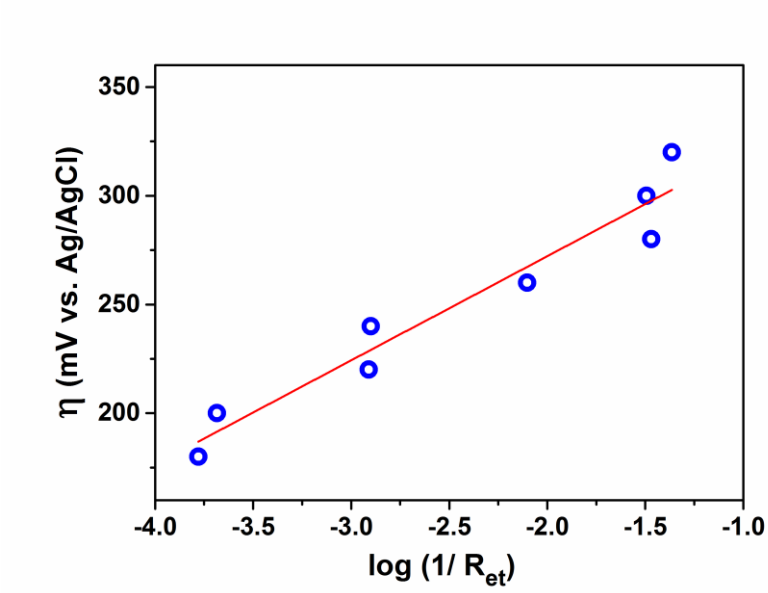

Figure 15. Tafel plot of Ru^0/CeO_2 (1.86% wt. Ru) modified GC electrode obtained using R_{et} from the electrochemical impedance analysis.

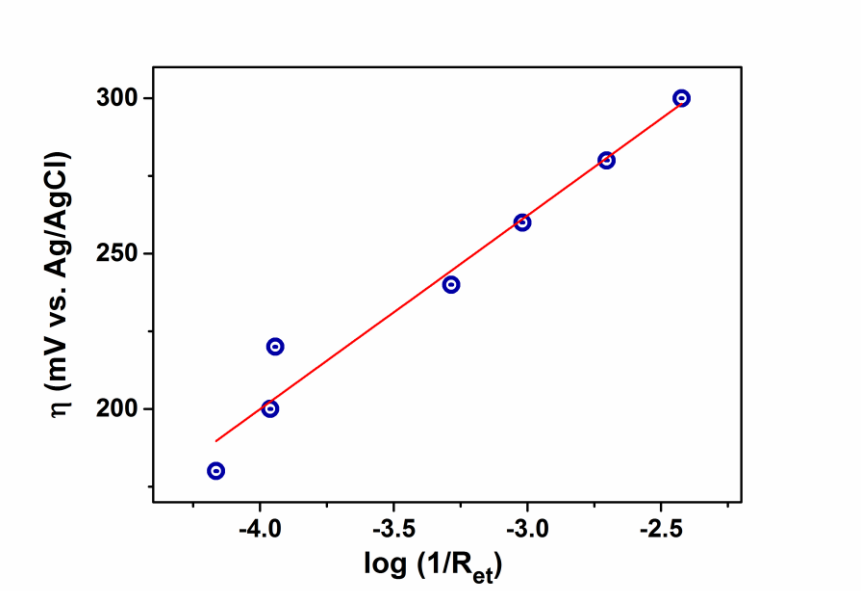

Figure 16. Tafel plot of Ru^0/TiO_2 (1.20% wt. Ru) modified GC electrode obtained using R_{et} from the electrochemical impedance analysis in 0.5 M H_2SO_4.

3.3. Comparison of Electrocatalytic Activity of Ru^0/CeO_2 on GC at Different Loading Level and Bare GC Electrodes in 0.5 M H_2SO_4 for HER

After determining the best metal oxide, different loading levels of Ru^0/CeO_2 modified GC electrodes were prepared and analyzed towards hydrogen evolution reaction during water electrolysis. To evaluate the electrocatalytic HER activity of modified electrodes, Ru^0/CeO_2 samples at different ruthenium loadings were loaded onto GC electrode (d = 3.00 mm) with a fixed mass loading (≈ 0.197 $mg.cm^{-2}$) by drop casting. It is noteworthy that required amount of the Ru^0/CeO_2 samples (see Table 4) was added on GCEs to maintain the same amount of ruthenium content on the modified electrode. The HER performances were measured in 0.5 M H_2SO_4 solution via linear sweep voltammetry (LSV). Polarization curves obtained by using Ru^0/CeO_2 modified electrodes at different ruthenium loadings are given in Figure 17a together with the one obtained by GCE without catalyst. Onset potentials for the modified electrodes shows slight variation for each Ru^0/CeO_2 samples at different ruthenium loading (Table 9 and Figure 17a).

Ru^0/CeO_2 catalysts with a ruthenium loading of 1.86% wt. modified GC electrode provides the lowest onset value (33 mV) as compared to the ones obtained by the other Ru^0/CeO_2 samples (Table 4). Indeed, it is even comparable to the Pt onset potential (1 mV) [50]. The overpotential values of the Ru^0/CeO_2 samples with different ruthenium loadings were also given in Table 9 for comparison. Among the catalyst modified GCEs given in Table 9 (note that all data were recorded without iR compensation), Ru^0/CeO_2 (1.86% wt. Ru) modified GCE needs the lowest overpotential (η) value to reach a current density (j) of 10 $mA.cm^{-2}$ (η = 47 mV) and 20 $mA.cm^{-2}$ (η = 65 mV). The over potential values of ceria based catalysts is found to be lower than the ones obtained by most of the other reported catalysts (in Table 2) such as Ni_2P (η = 130 mV at 20 $mA.cm^{-2}$) [80], CoP nanowire (η = 100 mV at 20 $mA.cm^{-2}$) [1], WS_2/RGO (η = 292 mV at 20 $mA.cm^{-2}$) [66], CoS|P/CNT (η = 65 mV at 20 $mA.cm^{-2}$) [68] (All data are given with respect to the RHE).

Table 9. The onset potentials and over potentials determined at various current densities for the Ru^0/CeO_2 modified glassy carbon electrodes at different ruthenium loadings.

Ru loading (% wt.)	**Onset (mV vs. RHE)**	**η (mV) at 5 $mA.cm^{-2}$**	**η (mV) at 10 $mA.cm^{-2}$**	**η (mV) at 15 $mA.cm^{-2}$**	**η (mV) at 20 $mA.cm^{-2}$**	**η (mV) at 25 $mA.cm^{-2}$**
0.92	42	45	61	73	81	89
1.86	33	37	47	55	65	72
2.98	44	47	65	77	89	99
3.95	45	49	67	76	87	97
4.90	40	45	61	71	81	91
5.96	42	49	65	75	85	95

Tafel slope (Figure 17b) and exchange current density (Figure 17c) values of the Ru^0/CeO_2 modified glassy carbon electrodes at different ruthenium loadings were also evaluated from linear sweep voltammograms using Tafel equation [3] ($\eta = a + b\log j$, where j is the current density, b is the Tafel slope and a is the exchange current density, j_0). Tafel slope values were found to be 49.89 $mV.dec^{-1}$, 41.18 $mV.dec^{-1}$, 50.84 $mV.dec^{-1}$, 48.04 $mV.dec^{-1}$, 48.49 $mV.dec^{-1}$ and 48.22 $mV.dec^{-1}$ for Ru^0/CeO_2 samples with a ruthenium loading of 0.92% wt., 1.86% wt., 2.98% wt., 3.95% wt., 4.90% wt. and 5.96% wt., respectively. These values indicate that electrochemical desorption process is the rate-limiting step and Volmer−Heyrovsky mechanism [34] is responsible for HER on the modified electrodes. On the other hand, the exchange current density values of these catalysts were determined as 0.61 $mA.cm^{-2}$, 0.67 $mA.cm^{-2}$, 0.61 $mA.cm^{-2}$, 0.47 $mA.cm^{-2}$, 0.60 $mA.cm^{-2}$, 0.51 $mA.cm^{-2}$ for the ruthenium loading of 0.92% wt., 1.86% wt., 2.98% wt., 3.95% wt., 4.90% wt. and 5.96% wt., respectively (see Figure 17c). The comparison of the Tafel slope and exchange current density values of these catalysts indicate that Ru^0/CeO_2 with a ruthenium loading of 1.86% wt. is an ideal catalyst for HER due to its lower Tafel slope and higher exchange current density values among the Ru^0/CeO_2 samples.

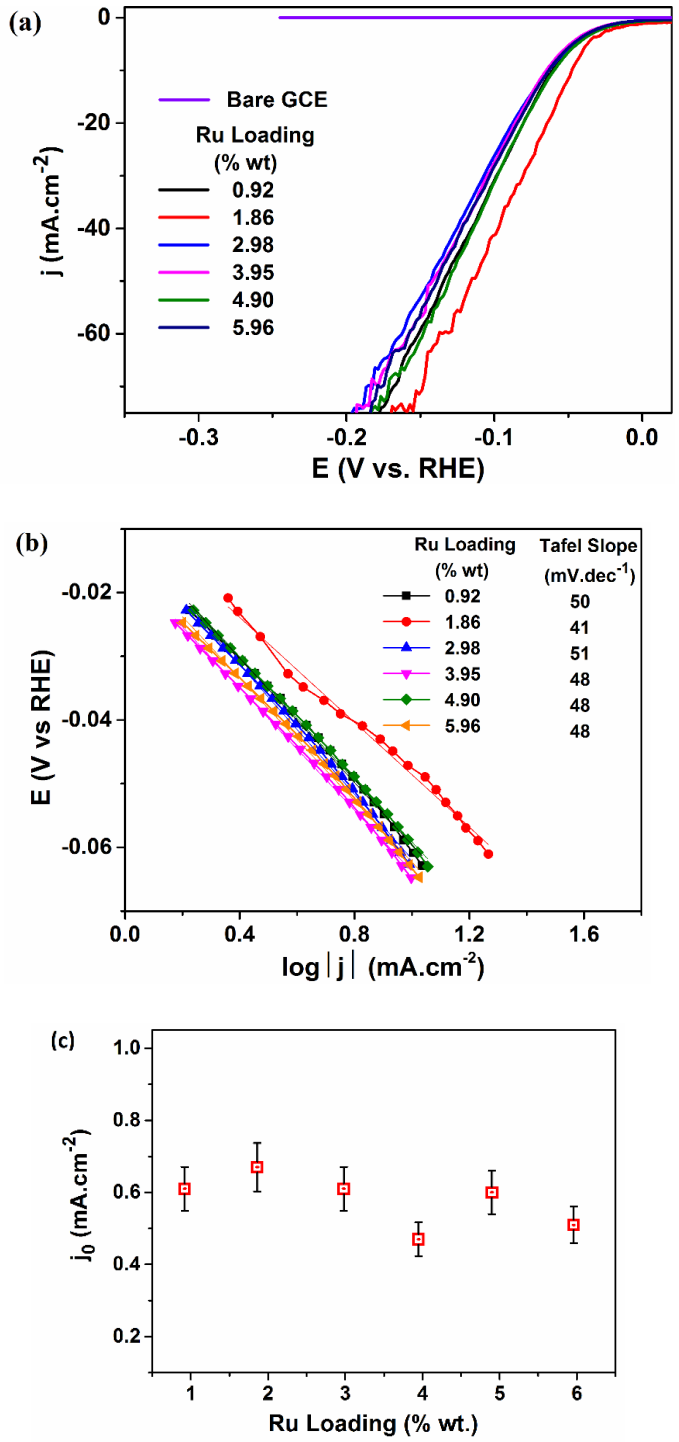

Figure 17. (a) Polarization curves of bare GCE and the Ru^0/CeO_2 samples with different ruthenium loadings on GCEs in 0.5 M H_2SO_4 at a scan rate of 5 $mV.s^{-1}$, **(b)** The corresponding Tafel plots obtained from polarization curves for HER, **(c)** The corresponding exchange current density of each electrocatalysts for HER.

The Tafel slope value of Ru^0/CeO_2 (1.86% wt. Ru) catalyst is lower than most of the reported catalysts given in Table 2 in 0.5 M H_2SO_4 such as Ru-MoO_2/GCE (S-2) (44 $mV.dec^{-1}$) [74], Ru nanosheet (46 $mV.dec^{-1}$) [43], Commercial Ru/Carbon (72 $mV.dec^{-1}$) [79], Ru/SiNWs (81 $mV.dec^{-1}$) [88], Ni_2P (46 $mV.dec^{-1}$) [80], WS_2NDs (51 $mV.dec^{-1}$) [2], N-WS_2-H_2 (70 $mV.dec^{-1}$) [48], WS_2 nanosheets (70 $mV.dec^{-1}$) [64], CoP nanowire (51 $mV.dec^{-1}$) [1] etc. In addition, Mo_2C/CNT (55.2 $mV.dec^{-1}$) [83] and β-Mo_2C (120 $mV.dec^{-1}$) [89] in 0.1 M $HClO_4$ and long Ru-TiNT (70 $mV.dec^{-1}$) [86] in 1.0 M $HClO_4$. Furthermore, Ru^0/CeO_2 (1.86% wt. Ru) provides higher exchange current density in HER as compared to other reported catalysts such as WS_2 nanodots (0.11 $mA.cm^{-2}$) [2], N-WS_2-H_2 (0.174 $mA.cm^{-2}$) [48], CoP nanowire (0.288 $mA.cm^{-2}$) [1] and Pt_2Si (0.33 $mA.cm^{-2}$) [68] (Table 2).

However, the comparison of the Tafel slope values and exchange current densities of the reported catalysts listed in Table 2 shows that there is no clear insight explaining the high activity of the catalysts according to the type of active metal nanoparticles. Indeed, the choice of the suitable supporting material seems to be critical as well as the active metal on the modified electrodes. Furthermore, there is no clear relation between Tafel slope value, onset and overpotentials of the reported catalysts (Table 2). For example, among the ruthenium based catalysts, the lowest onset potential (3 mV) was achieved by Ru/GLC [79] which provide Tafel slope of 46 $mV.dec^{-1}$ with an overvoltage of 35 mV at j=10 $mA.cm^{-2}$ while Ru@C_2N catalyst [50] provides the lowest Tafel slope (30 $mV.dec^{-1}$) with onset and overpotentials of 9.5 mV and 22 mV at j=10 $mA.cm^{-2}$.

Table 10. The overpotentials determined to reach various TOF values for Ru^0/CeO_2 (1.86% wt. Ru) modified GC electrode together with recently reported catalysts.

Catalyst	η (mV vs. RHE)	TOF, s^{-1}	Ref.
Ru^0/CeO_2 (1.86% wt. Ru)	23.67 26.27 28.30	0.67 0.725 0.80	This Work
CoP	82.00	0.80	96
$Ru@C_2N$	25.00	0.67	50
$N\text{-}WS_2\text{-}H_2$	108	0.725	48
Pt	0.00	0.80	96

The turnover frequency (TOF) values of Ru^0/CeO_2 (1.86% wt. Ru) catalyst which was calculated as described in the experimental part (See Part 2.5.3 d) by recording CV of Ru^0/CeO_2 (1.86% wt. Ru) modified GCE in 1.00 M phosphate buffer saline solution (PBS, pH= 7.4) in the potential range of -0.5 to + 0.6 V vs. Ag/AgCl at a scan rate of 50 $mV.s^{-1}$. As expected, Pt with a TOF value of 0.8 s^{-1} at 0 V [96] exhibits the best HER catalytic activity among the reported catalysts. Ru^0/CeO_2 (1.86% wt. Ru) modified GCE provides a TOF value of 0.8 s^{-1} which could be achieved at η = 28 mV (as seen in Table 10). Indeed, this overpotential value is lower than most of the reported modified electrodes such as CoP nanocatalyst (required overpotential is 82 mV to reach a TOF value of 0.8 s^{-1}) [96], $N\text{-}WS_2\text{-}H_2$ (required overpotential is 108 mV to reach a TOF value of 0.725 s^{-1}) [48], $Ru@C_2N$ modified electrode needs an overpotential of 25.00 mV to achieve a TOF value of 0.670 s^{-1} [50].

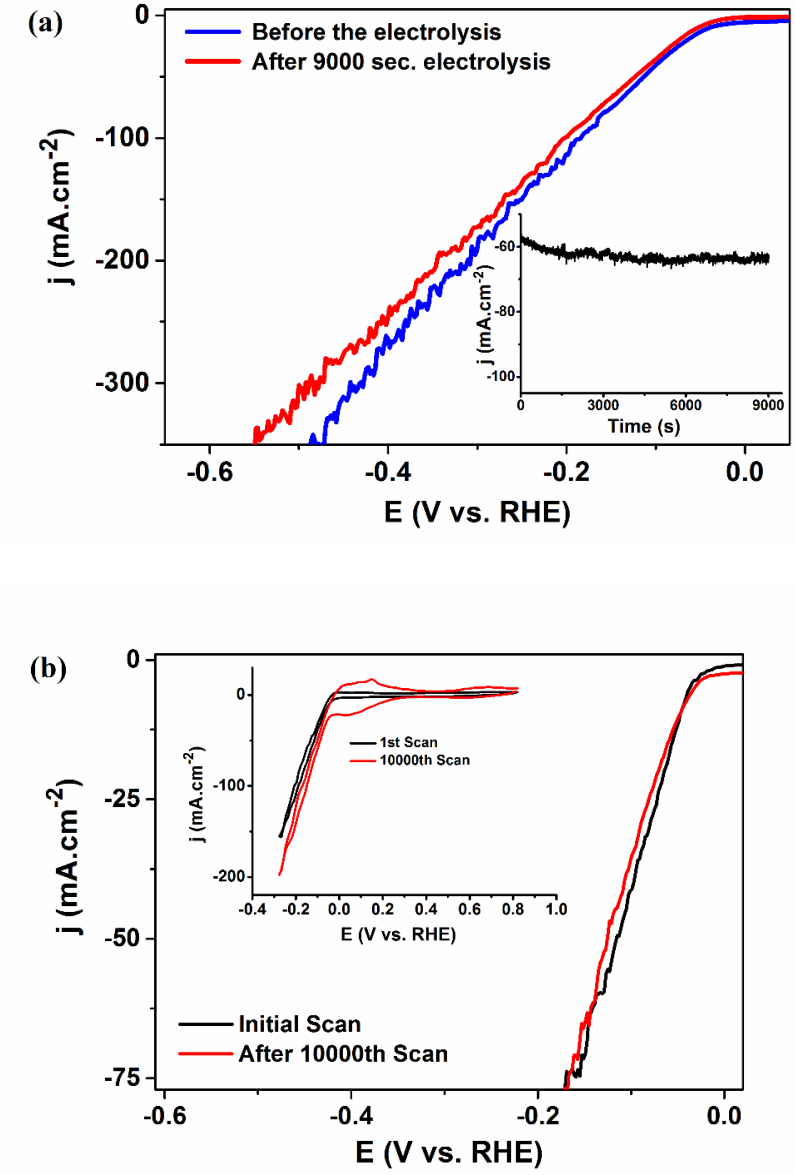

Figure 18. **(a)** The polarization curves of the Ru^0/CeO_2 (1.86% wt. Ru) modified GCE before and after stability test in 0.5 M H_2SO_4 (Inset: variation of current density during chronoamperometric electrolysis) **(b)** The polarization curves of Ru^0/CeO_2 (1.86% wt. Ru) modified GCE before and after 10,000 CV cycles in 0.5 M H_2SO_4 (Inset: CV measurement within the range of (-0.3V) - (0.8 V) vs. RHE

Catalytic stability test for Ru^0/CeO_2 (1.86% wt. Ru) on GC electrode was also performed. In this test, the modified electrode subjected to constant potential electrolysis at an overpotential of -350 mV vs. Ag/AgCl for 9000 s in 0.5 M H_2SO_4 aqueous solution. The result shows that the current density of initial value stays nearly the same with the ones obtained after 9000 s (See the inset of Figure 18a). Polarization curves recorded before and after constant potential electrolysis given in Figure 18a shows that there is no change in onset potentials after 9000 s electrolysis. The stability of Ru^0/CeO_2 (1.86% wt. Ru) on GC electrode was also investigated by recording the voltammograms in the range of -0.50 to 0.60 V versus Ag/AgCl at a scan rate of 100 $mV.s^{-1}$ in 0.5 M H_2SO_4 aqueous solution. The comparisons of the cyclic voltammograms and the polarization curves recorded before and after 10,000 scans (Figure 18b) indicates that there is almost no change in onset potentials and current density. Indeed, Ru^0/CeO_2 (1.86% wt. Ru) on GC electrode provides outstanding electrocatalytic stability in HER as compared to the reported catalysts such as Ni_2P [80] (exhibits 25 mV negative shift at a current density of 10 $mA.cm^{-2}$ after 500 scans), Mo_2C/CNT [83] (exhibits ≈ 14 mV negative shift at a current density of 10 $mA.cm^{-2}$ after 3000 scans), Pt/C [50] and CoMoP@C [101] (exhibit more than 47 mV negative shift and ≈ 20 mV negative shift at a current density of 10 $mA.cm^{-2}$ after 10,000 scans, respectively).

To determine HER activity of catalyst, the amount of hydrogen release was measured for both modified GC and Pt electrodes in a Hoffman electrolysis apparatus in 0.5 M H_2SO_4 aqeous solution. Constant current of 5 mA was applied to the electrode at room temperature and the volume of H_2 released was monitored as a function of time and the results are given in Figure 19 together with the teoretical amount of H_2 released for comparison. After the delivery of 3000 mC of charge, the Faradaic yield of the modified electrode, Ru^0/CeO_2 (1.86% wt. Ru) on GCE, for H_2 production was detected as nearly same as theoretical value (> 95%) (Figure 19). In literature, there are few reports measuring the amount of H_2 production during the electrolysis. For example, the faradaic yield of H_2 production by $Co_{0.6}Mo_{1.4}N_2$ electrocatalyst [102] after delivery of 30 Coulombs of charge was determined as > 90% and after delivery of 100

Coulombs of charge, the Faradaic yield of CoP/Ti [65] working electrode was found as ≈ 100% for HER.

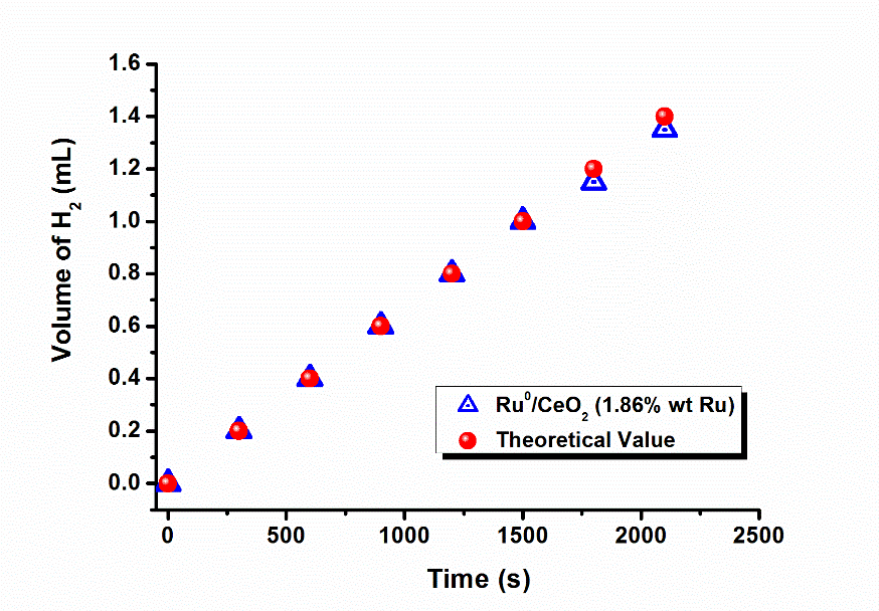

Figure 19. Volume of H_2 versus time graph during the galvonastatic electrolysis HER using Ru^0/CeO_2 (1.86% wt. Ru) modified GC electrode in 0.5 M H_2SO_4.

3.4.Comparison of Electrocatalytic Activity of Ru^0/MO_2 (M= Ti, Zr, Hf, Ce) on GC and Bare GC Electrode in KOH Solution for OER

Ru^0/MO_2 modified electrodes were also tested for OER by recording polarization curves in the range of 0.0 to +1.7 V vs. Ag/AgCl in 0.5 M KOH solution. The resulting polarization curves are given in Figure 20 together with polarization curve for GC electrode recorded in the same medium. An inspection of Figure 20 reveals that Ru^0/CeO_2 modified GC electrode has the lowest overpotential value (302 mV) among the four Ru^0/MO_2 (M = Ti, Zr, Hf, Ce) modified GC electrodes. The onset potentials and overpotential values at a certain current density of the Ru^0/MO_2 samples were also given in Table 11 (note that all data were recorded without iR compensation) for comparison. Ru^0/CeO_2 (1.86% wt. Ru) modified GC electrode needs the lowest overpotentials (η) value to reach any defined current densties, for instance, the

overpotentials at current densities (j) of 10 mA.cm^{-2} and (j) of 20 mA.cm^{-2} was found to be 425 mV and ɳ = 530 mV, respectively. On the other hand, Ru^0/TiO_2, Ru^0/ZrO_2, Ru^0/HfO_2 modified GC electrodes produce anodic current density (j) of 20 mA.cm^{-2} at ɳ = 1.21 V, ɳ = 1.18 V, ɳ = 1.24 V, respectively. Ru^0/CeO_2 (1.86% wt. Ru) on GC electrode is comparable to the behavior of other OER electrocatalysts, for instance, the overpotential at 20 mA.cm^{-2} was found to be 487 mV for CoO_x /Au [103] and 480 mV for Fe–Co_3O_4@Fe-Co-Bi [69], also the overpotential at 10 mA.cm^{-2} was found to be 350 mV for CP@FeP [104] and 453 mV for CoO_x /Au [103] in alkaline solutions. (Others are tabulated in Table 12) However, there are few examples of bifunctional catalysts and, thus, designing of efficient catalyst for both HER and OER reaction is very attractive issue.

Table 11. The onset potentials and the overpotentials versus RHE at various current densities for the Ru^0/MO_2 (M= Ti, Zr, Hf, Ce) modified glassy carbon electrodes in 0.5 M KOH.

Ru^0/MO_2 - GCE	**Onset (V vs. RHE)**	**ɳ (V) at 5 mA.cm^{-2}**	**ɳ (V) at 10 mA.cm^{-2}**	**ɳ (V) at 15 mA.cm^{-2}**	**ɳ (V) at 20 mA.cm^{-2}**
Ru^0/TiO_2 (1.20% wt. Ru)	0.85	0.984	1.094	1.154	1.214
Ru^0/ZrO_2 (1.41% wt. Ru)	0.81	0.974	1.084	1.144	1.184
Ru^0/HfO_2 (2.00% wt. Ru)	0.74	0.864	0.984	1.174	1.244
Ru^0/CeO_2 (1.86% wt. Ru)	0.29	0.357	0.425	0.481	0.530

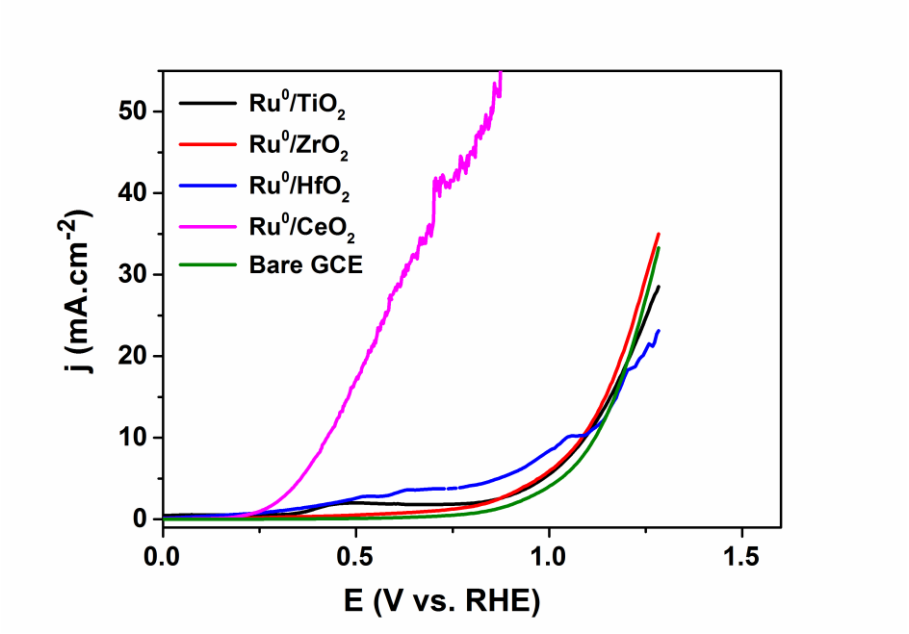

Figure 20. Polarization curves of bare GCE and the Ru^0/MO_2 (M= Ti, Zr, Hf, Ce) modified GCEs in 0.5 M KOH at a scan rate of 5 $mV.s^{-1}$.

It is commonly acceptable to express potential in terms of the oxygen overpotential, η, $\eta = E_{irr} - E_{rev}$, where, E_{irr} is the irreversible electrode potential (the measured electrode potential, E_{meas}) and E_{rev} is the reversible electrode potential. It is worthy to note that when the reference electrode is normal hydrogen electrode (NHE) in alkaline solution needed potential to produce to O_2 is ($E_{rev} = 1.23 – 0.059$ pH), 0.404 V vs. NHE at pH= 14 (as shown in Equation 5). However, if Ag/AgCl electrode is used instead of NHE in the same solution, E = 0.207 V is needed. Therefore, in this case overpotential is related to the potential, E_{meas}, measured on the Ag/AgCl and NHE scale at pH= 14 as following Equation (10) and (11): [103]

$$\eta = E_{meas} - 0.207\ V \qquad (10)$$

$$\eta = E_{meas} - 0.404\ V \qquad (11)$$

Table 12. Summary of some recently reported representative OER electrocatalysts in alkaline electrolytes. Data were recorded [a] without and [b] with iR compensation (i: Current, R: Resistance)

Catalyst	Catalysis Condition	Loading density (μg. cm^{-2})	Tafel Slope (mV. dec^{-1})	j (mA. cm^{-2})	η (mV) at defined j	Ref.
Ru oxide nanosheet [b]	0.5 M H_2SO_4	100	54	10 mA.mg^{-1}	260	43
NiSe/NF	1.0 M KOH	2800	64	20	270	73
CP@FeP [b]	1.0 M KOH	--	64	10 20	350 390	104
Ru^0/CeO_2 [a] (1.86% wt. Ru)	0.5 M KOH	197	150	5 10 20	357 425 530	This Work
Fe–Co_3O_4@Fe–Co–Bi [b]	0.1 M K-Bi (pH=9.2)	1320	121	5 10 20	384 420 480	69
CoO_x/Au	0.5 M KOH	--	120	5 10 20	423 453 487	103
MnO_2/$NiCo_2O_4$/NF	1.0 M KOH	--	139	10	340	105

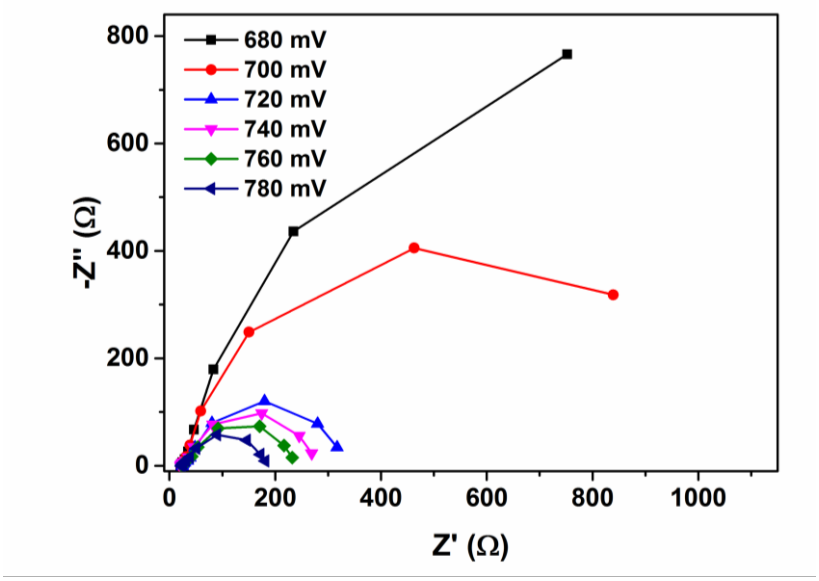

Figure 21. The Nyquist plots for Ru^0/CeO_2 (1.86% wt. Ru) modified GC electrode at different overpotentials just before onset and after onset potential versus Ag/AgCl in 0.5 M KOH.

In order to determine the catalytic activity of Ru^0/CeO_2 (1.86% wt. Ru) on GC electrode for the OER in 0.5 M KOH, EIS analysis was also performed at various overpotentials vs. Ag/AgCl. The representative Nyquist plots (Figure 21) for Ru^0/CeO_2 (1.86% wt. Ru) on GC electrode at different overpotentials consist of a small semicircle in the high frequency region due to porous surface of modified electrodes and a larger semicircle in the high frequency region due to electron transfer reaction. These data were modeled by the electrical equivalent circuit, and the diameter of the semicircles decreases with the increasing specific overpotentials indicating the decrease in electron transfer resistance, R_{et}.

Tafel slope was also evaluated from the EIS data by plotting log (1/ R_{et}) versus overpotential value (Figure 22) and found to be 83 $mV.dec^{-1}$. This value, contrary to the values obtained for HER, was found to be different from the one obtained from the LSV (140 $mV.dec^{-1}$). Furthermore, R_{et} values were also used to evaluate the exchange current densities (j_o) at each overpotential value (η) by using Equation 9. As expected,

there is an increase in the exchange current densities with the increase in the overpotential values (See Table 13).

Table 13. Exchange current densities (j_0) and electron transfer resistances (R_{et}) of Ru^0/CeO_2 (1.86% wt. Ru) modified GC electrode with respect to potential.

E (mV vs. Ag/AgCl)	R_{et} (Ω)	j_0 (mA.cm^{-2})
680	2050	0.179
700	1078	0.340
720	341	1.076
740	265	1.385
760	220	1.668
780	192	1.912

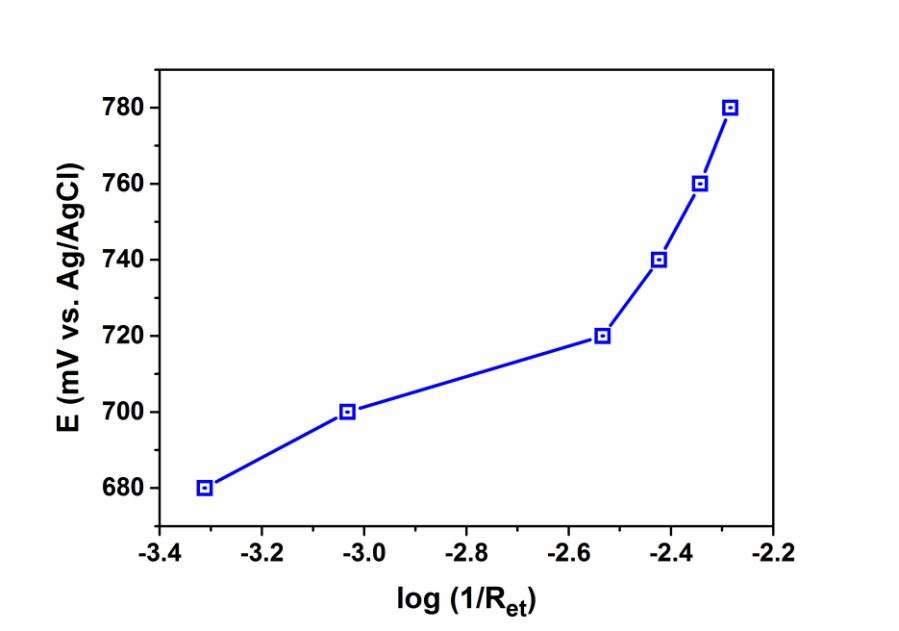

Figure 22. Tafel plot of Ru^0/CeO_2 (1.86% wt. Ru) modified GC electrode obtained using R_{et} from the electrochemical impedance analysis in 0.5 M KOH.

For testing the effect of KOH concentration on the OER, the linear sweep voltammetry (LSV) curves for the Ru^0/CeO_2 (1.86% wt. Ru) coated GC electrode were recorded in various KOH concentrations, as an example, Figure 23 shows four typical LSV curves recorded in 0.1, 0.5, 1.0 and 3.0 M KOH, respectively. KNO_3 was added to maintain a constant concentration (3.0 $mol.dm^{-3}$) of cations and anions in the solution. The LSV curves shown in Figure 23 indicate that current densities increase with increasing KOH concentration in the entire studied potential range. Furthermore, Tafel slope of Ru^0/CeO_2 is nearly independent of KOH concentration, this means that the reaction mechanism of the OER stays same within the all KOH concentration.

The reaction order in OH^- concentration was determined by measuring the slope of the plot log j vs log c_{OH^-} and found as nearly 1 at just before (0.7 V vs. Ag/AgCl) and after the onset potential (0.8 V vs. Ag/AgCl) of Ru^0/CeO_2-GC electrode and a close linear relationship was observed as shown in Figure 24. The slope of the plot, which is the reaction order of the OER with respect to KOH, was found to be same at low potentials (e.g. 0.70 V) and at high potentials (e.g. 0.80 V).

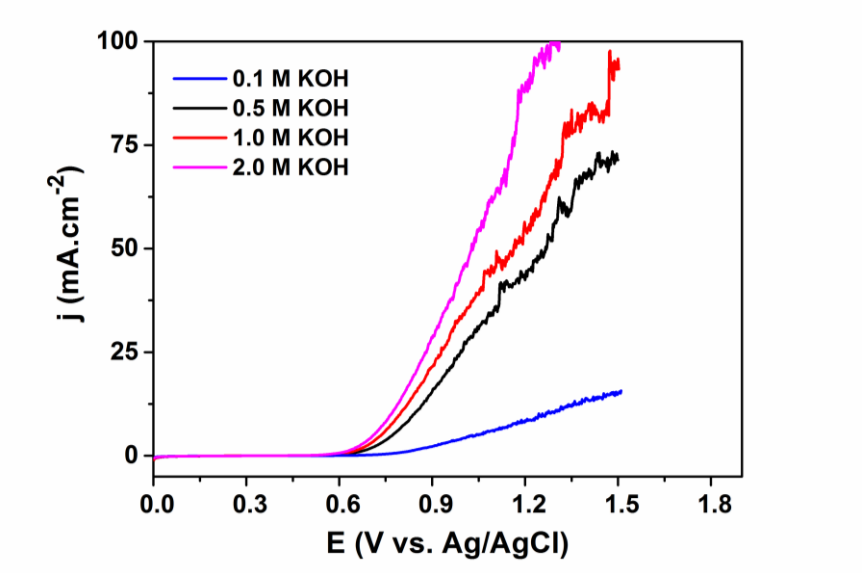

Figure 23. Polarization curves recorded using a GC electrode coated by Ru^0/CeO_2 (1.86% wt. Ru) catalyst in alkaline solutions with four different KOH concentrations as marked. The electrode potential scan rate: 5 $mV.s^{-1}$.

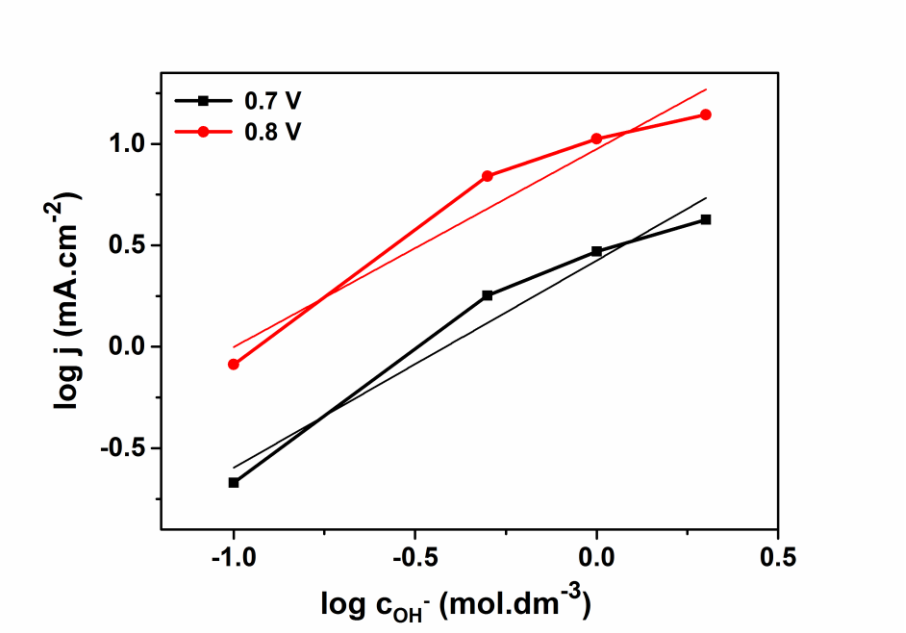

Figure 24. log j versus log c_{OH^-} plot for Ru^0/CeO_2 (1.86% wt. Ru) modified GCE at different constant potentials at room temperature.

CHAPTER 4

CONCLUSIONS

In summary, nanotitania, nanozirconia, hafnia(IV) oxide, and nanoceria, supported ruthenium(0) nanoparticles were successfully prepared by the impregnation of Ru^{3+} ions on the surface of ceria followed by the sodium borohydride reduction of Ru^{3+} ions in aqueous solution at room temperature. Characterization of the synthesized catalysts were done by using TEM, ICP-OES, XRD, EDX and XPS. A highly efficient HER from water at room temperature was achieved using Ru^0/MO_2 (M= Ti, Zr, Hf, Ce) on glassy carbon electrode at same mass loading level (≈ 0.197 mg.cm^{-2}) by drop casting.

Electrochemical behavior of the modified glassy carbon electrodes and their electrocatalytic activity towards the hydrogen evolution during water electrolysis was investigated in acidic solution (0.5 M H_2SO_4) at room temperature by linear sweep voltammetry (LSV), cyclic voltammetry (CV), potentiostatic electrochemical impedance spectroscopy (EIS) and constant potential electrolysis. Among the Ru^0/MO_2 modified GCEs, Ru^0/CeO_2 on GCE was found to be better for HER in terms of onset potentials, current density at a defined overpotential, exchange current densities and Tafel slopes.

As well as determining best metal oxides for HER, loading level effect was also investigated. Ru^0/CeO_2 (1.86% wt. Ru) modifed GC electrode was found to be better than the other loading levels of Ru^0/CeO_2 for HER. Electrochemical behavior of the modified electrodes were investigated by linear sweep voltammetry. The catalyst provided an overpotential of 47 mV (at j= 10 mA.cm^{-2}) with a low onset value (33 mV) in HER. In addition, very low Tafel slope value of 41 mV.dec^{-1} was obtained with a high exchange current density of 0.67 mA.cm^{-2}. More importantly, Ru^0/CeO_2 with a

1.86% wt. Ru was found to be highly stable electrocatalysts used for HER in acidic water splitting. Indeed, no noticeable change in the exchange current density was observed even after the 10,000 scans. Moreover, it shows excellent stability/durability in acidic solution for a long-term constant (9000 seconds) potential electrolysis. In addition to this, the Faradaic yield of modified electrodes for H_2 production was detected as nearly same as theoretical value (>95%).

Furthermore, electrochemical behavior of Ru^0/MO_2 modified GCEs and their electrocatalytic activity towards the oxygen evolution reaction during water electrolysis was investigated in alkaline electrolyte (0.5 M KOH). Ru^0/CeO_2 (1.86% wt. Ru) on GC electrode has the best catalytic activity towards OER because it has low onset potential and needs lowest overpotential to reach a defined current density.

REFERENCES

[1] Tian J., Liu Q., Asiri A., Sun X., J. Am. Chem. Soc. 136 (2014) 7587-7590.

[2] Zhao X., Ma X., Sun J., Li D., Yang X., ACS Nano 10 (2016) 2159-2166.

[3] Zou X., Zhang Y., Chem. Soc. Rev. 44 (2015) 5148-5180.

[4] Morales-Guio C., Stern L., Hu X., Chem. Soc. Rev. 43 (2014) 6555-6569.

[5] Atkins P., De Paula J., Atkins' Physical chemistry, Oxford University Press, Oxford, 2006.

[6] Moulijn J. A., Van Leeuwen P. W. N. M., Van Santen R. A., Catalysis: An Integrated Approach to Homogeneous, Heterogeneous and Industrial Catalysis. Elsevier Science Publishers, the Netherlands, 1993.

[7]Carberry J., Chemical and catalytic reaction engineering, N.Y.: Dover Publications, Mineola, 2001.

[8] Richards R. M., Surface and Nanomolecular Catalysis, Taylor & Francis, Boca Raton, 2006.

[9] Sullivan J. A., Flanagan K. A., Hain H., Catal. Today, 145 (2009) 108-113.

[10] Ma L., Wang J., Wang H., Zhang Q., Lu C., He X., Li X., Chin. J. Chem. Eng., 25 (2017) 306-312.

[11] Ashouri F., Zare M., Bagherzadeh M., C. R. Chimie, 20 (2017) 107-115.

[12] Li X., Zhang B., Wu Q., Zhang C., Yu Y., Li Y., Lin W., Cheng H., Zhao, F., J. Catal., 337 (2016) 284-292.

[13] Selvaraj V., Vinoba M. and Alagar M., J. Colloid Interface Sci., 322 (2008) 537-544.

[14] Brook M. A., Ketelson H. A., LaRonde F. J., Pelton R., Inorganica Chimica Acta, 264 (1997) 125-135.

[15] Michel C. G., Bambrick W. E., Ebel R. H., Fuel Process. Technol., 35 (1993) 159-182.

[16] Aiken J. D.and Finke R. G., J. Mol. Catal. A: Chem., 145 (1999) 1-44.

[17] Pachon L. D., Thathagar M. B., Hartl F.,Rothenberg G., RSC Phys. Chem. Chem. Phys., 8 (2008) 151-157.

[18] Hayashi Y., Inoue M., Takizawa H., Suganuma K., Nanopackaging: Nanotechnologies and Electronics Packaging, Springer Science and Business Media, New York, 2008.

[19] Y. Tonbul, S. Akbayrak, S. Özkar, Int. J. Hydrogen Energy 41 (2016) 11154-11162.

[20] Y. Cheng, P. Jiangn, Prog. Nat. Sci-Mater. 25 (2015) 545–553.

[21] S. Akbayrak, Y. Tonbul, S. Özkar, Dalton Trans. 45 (2016) 10969–10978.

[22] Gao H., Xiao F., Ching C. B., Duan H., ACS Appl. Mater. Interfaces, 3 (2011) 3049-3057.

[23] Zhu Q.-L., Li J., Xu Q. J. Am. Chem. Soc., 135 (2013) 10210-10213.

[24] Kraynov A., Müller T. E., Concepts for the Stabilization of Metal Nanoparticles in Ionic Liquids, Applications of Ionic Liquids in Science and Technology, InTech, Shangai, 2011.

[25] Polte J., RSC CrystEngComm, 17 (2015) 6809-6830.

[26] Hierrezuelo J., Sadeghpour A., Szilagyi I., Vaccaro A., Borkovec M., Langmuir, 26 (2010) 15109-15111.

[27] Çelik, D., Rhodium(0) Nanoparticles supported on Hydoxyapatite: Preparation, Characterization and Catalytic Use in Hydrogen Generation From Hydrolysis of

Hydrazine Borane and Ammonia Borane, Master of Science Thesis in Chemistry, METU, Ankara, 2012.

[28] Elbasuney S., Appl. Surf. Sci., 409 (2017) 438-447.

[29] Cao G., Nanostructures & nanomaterials: Synthesis, properties and applications, Imperial College Press, London, 2004.

[30] Napper, D.H., In Polymeric Stabilization of Colloidal Dispersions, Academic Press, London, UK, 1983.

[31] Rahman S. M., Miah M. D., Renew. Sust. Energy Rev., 74 (2017) 110-115.

[32] McAuliffe, C. A., Hydrogen and Energy, The Macmillan Press Ltd, Hong Kong, 1980.

[33] Sørensen, B., Hydrogen and fuel cells, Elsevier, Amsterdam, 2012.

[34] Liu W., Hu E., Jiang H., Xiang Y., Weng Z., Li M., Fan Q., Yu X., Altman E. I., Wang H., Nat. Commun. 7 (2016) 10771-10780.

[35] Liu Y., Yu G., Li G-D., Sun Y., Asefa T., Chen W., Zou X., Angew. Chem. Int. Ed. 54 (2015) 10752-10757.

[36] Turner, J. A., Science, 285 (1999) 687-689.

[37] Ismail, A. A., Bahnemann, D. W., Sol. Energy Mater. Sol. Cells, 128 (2014) 85-101.

[38] Grimes A. C., Varghese K. O., Ranjan S., Light, Water, Hydrogen - The Solar Generation of Hydrogen by Water Photoelectrolysis, Springer Science, New York, 2008.

[39] Gupta, R. B., Hydrogen Fuel- Production, Transport and Storage, CRC Press, Boca Raton, 2009.

[40] Lu T., Chen C., Basu M., Ma C. G., Liu R. S., Chem. Commun. 51 (2015) 17012-17015.

[41] Kanan M. W., Nocera D. G., Science, 321, (2008) 1072-1075.

[42] Tahir M., Pan L., Idrees F., Zhang X., Wang L., Zou J.-J., Wang, Z. L., Nano Energy, 37, (2017). 136-157.

[43] Kong X., Xu K., Zhang C., Dai J., Oliaee S. N., Li L., Zeng X., Wu C., Peng Z., ACS Catal. 6 (2016) 1487–1492.

[44] Wu J., Xue Y., Yan X., Yan W., Cheng Q., Xie Y., Nano Res., 5 (2012) 521-530.

[45] Patel P. P., Datta M. K., Velikokhatnyi O. I., Kuruba R., Damodaran K., Jampani P., Gattu B., Shanthi P. M., Damle S. S., Kumta P. N. Sci. Rep., 6 (2016) 28367.

[46] Smith A. M., Trotochaud L. , Burke M. S., Boettcher S. W., RSC Chem. Commun., 51 (2015) 5261-5263.

[47] Leeuwen, P., Homogeneous catalysis, Science Press, Beijing, 2008.

[48] Sun C., Zhang J., Ma J., Liu P., Gao D., Tao K., Xue D., J. Mater. Chem. A, 4 (2016) 11234-11238.

[49] Yan Y., Xia B., Xu Z., Wang X., ACS Catal., 4 (2014) 1693-1705.

[50] Mahmood J., Li F., Jung S. M., Okyay M. S., Ahmad I., Kim S. J., Park N., Jeong H.Y., Baek J. B., Nat. Nanotechnol. 12 (2017) 441–446.

[51] Artero V., Chavarot-Kerlidou M., Fontecave M., Angew. Chem. Int. Ed., 50 (2011) 7238-7266.

[52] Akhtar A., Ghaffarinejad A., Milani Hosseini S. M. R., Manteghi F., Maminejad N., J. Electroanal. Chem., 739 (2015) 73-83.

[53] Merki D., Fierro S., Vrubel H., Hu X. Chem. Sci., 2 (2011) 1262-1267.

[54] Chen W.-F., Wang C.-H., Sasaki K., Marinkovic N., Xu W., Muckerman J. T., Zhu Y., Adzic R. R., Energy Environ. Sci. 6 (2013) 943-951.

[55] Chelucci G., Baldino S., Baratta W., Coord. Chem. Rev., 300 (2015) 29-85.

[56] McFarland E., Science, 338 (2012), 340-342.

[57] Jones D. R., Iqbal S., Kondrat S. A., Lari G. M., Miedziak P. J., Morgan D. J., Parker S. F., Hutchings G. J., Phys. Chem. Chem. Phys. 18 (2016) 17259-17264.

[58] Kusada K., Kobayashi H., Yamamoto T., Matsumura S., Sato K., Nagaoka K., Kubota Y., Kitagawa H., J. Am. Chem. Soc. 135 (2013) 5493-5496.

[59] Akbayrak S., Tonbul Y., Özkar S., Appl. Catal. B 198 (2016) 162–170.

[60] Kalkan E., Akbayrak S. and Özkar S., J. Mol. Catal. A: Chem, 430 (2017) 29-35.

[61] Dole H.A.E., Safady L.F., Ntais S., Couillard M., Baranova E.A., J. Catal. 318 (2014) 85–94.

[62] Anderson J.M., Mcinnis M.D., Malhotra A., Zhai L., Mater. Express, 3 (2013) 11–20.

[63] Audichon T., Morisset S., Napporn T.W., Kokoh K. B., ChemElectroChem 2 (2015) 1128–1137.

[64] Lukowski M. A., Daniel A. S., English C. R., Meng F., Forticaux A., Hamers R. J., Jin S., Energy Environ. Sci. 7 (2014) 2608-2613.

[65] Popczun E. J., Read C. G., Roske C. W., Lewis N. S., Schaak R. E., Angew. Chem. Int. Ed. 53 (2014) 5427-5430.

[66] Yang J., Voiry D., Ahn S. J., Kang D., Kim A. Y., Chhowalla M., Shin H. S., Angew. Chem. Int. Ed. 52 (2013) 13751-13754.

[67] X. Huang, Z. Zeng, S. Bao, M. Wang, X. Qi, Z. Fan, H. Zhang, Nat. Commun. 4 (2013) 1444-1452.

[68] Zhu Y., Yuan M., Deng L., Ming R., Zhang A., Yang M., Chai B., Ren Z., RSC Adv. (2017) 1553-1560.

[69] Zhu G., Ge R., Qu F., Du G., Asiri A. M., Yao Y., Sun X., J. Mater. Chem. A, 5 (2017) 6388-6392.

[70] Shang X., Li X., Hu, W.-H., Dong B., Liu Y.-R., Han G.-Q., Chai Y.-M., Liu Y.-Q., Liu, C.-G., Appl. Surf. Sci., 378 (2016) 15-21.

[71] Singh D. K., Jenjeti R. N., Sampath S., Eswaramoorthy M., RSC J. Mater. Chem. A, 5 (2017) 6025-6031.

[72] Jiao L., Zhou Y.-X., Jiang H.-L., RSC Chem. Sci. 7 (2016) 1690-1995.

[73] Tang C., Cheng N., Pu Z., Xing W., Sun X., Angew. Chem. 127 (2015) 9483-9487.

[74] Jiang P., Yang Y., Shi R., Xia G., Chen J., Su J., Chen Q., J. Mater. Chem. A 5 (2017) 5475-5485.

[75] Kong D., Wang H., Lu Z., Cui Y., J. Am. Chem. Soc. 136 (2014) 4897-4900.

[76] Ma R., Zhou Y., Chen Y., Li P., Liu Q., Wang J., Angew. Chem. 127 (2015) 14936-14940.

[77] Zhang L-N., Li S-H., Tan H-Q., Khan S. U., Ma Y., Zang H., Wang Y., Li Y-Y., ACS Appl. Mater. Interfaces 9 (2017) 16270-16279.

[78] McEnaney J. M., Crompton J. C., Callejas J. F., Popczun E. J., Biacchi A. J., Lewis N. S., Schaak R. E., Chem. Mater. 26 (2014) 4826-4831.

[79] Chen Z., Lu J., Ai Y.-J., Ji Y., Adschiri T., Wan L., ACS Appl. Mater. Interfaces 8 (2016) 35132−35137.

[80] Popczun E. J., McKone J. R., Read C. G., Biacchi A. J., Wiltrout A. M., Lewis N. S., Schaak R. E., J. Am. Chem. Soc. 135 (2013) 9267-9270.

[81] Yan H., Tian C., Wang L., Wu A., Meng M., Zhao L., Fu H., Angew. Chem. Int. Ed. 54 (2015) 6325-6329.

[82] Zhu Y., Chen G., Xu X., Yang G., Liu M., Shao Z., ACS Catal. 7 (2017) 3540-3547.

[83] Chen W.-F., Wang C.-H., Sasaki K., Marinkovic N., Xu W., J. Muckerman T., Zhu Y., Adzic R. R., Energy Environ. Sci. 6 (2013) 943-951.

[84] Cabán-Acevedo M., Stone M. L., Schmidt J. R., Thomas J. G., Ding Q., Chang H-C., Tsai M.-L., He Jr.-H., Jin S., Nat. Mater. 14 (2015) 1245-1251.

[85] Zou X., Huang X., Goswami A., Silva R., Sathe B. R., Mikmeková E., Asefa T., Angew. Chem. Int. Ed. 126 (2014) 4461-4465.

[86] Lačnjevac U.Č., Radmilović V.V., Radmilović V.R., Krstajić N.V., Electrochim. Acta 168 (2015) 178-190.

[87] Döner A., Tezcan F., Kardaş G., Int. J. Hydrogen Energy 38 (2013) 3881-3888.

[88] Zhu L., Cai Q., Liao F., Sheng M., Wu B., Shao M., Electrochem.Commun. 52 (2015) 29-33.

[89] Wan C., Regmi Y., Leonard B., Angew. Chem. Int. Ed. 126 (2014) 6525-6528.

[90] Pi Y., Shao Q., Wang P., Guo J., Huang, X., Adv. Funct. Mater., 27 (2017) 1700886.

[91] Luo J., Im J., Mayer M., Schreier M., Nazeeruddin M., Park N., Tilley S., Fan H., Gratzel, M., Science, 345 (2014) 1593-1596.

[92] Lee J., Sher Shah S. A., Yoo P. J., Lim B., Chem. Phys. Lett., 673 (2017) 89-92.

[93] Skúlason E., Karlberg G. S., Rossmeisl J., Bligaard T., Greeley J., Jónsson H., Nørskov J., Phys. Chem. Chem. Phys., 9 (2007) 3241-3250.

[94] Sarabay-Reintjes A., Electrochim. Acta, 31 (1986) 251-254.

[95] Kozuch S. and Shaik S., Accounts of Chemical Research, 44 (2011) 101-110.

[96] Li J., Zhou X., Xia Z., Zhang Z., Li J., Ma Y., Qu Y., J. Mater. Chem. A, 3(2015) 13066-13071.

[97] Uygun, Z. O., Ertuğrul-Uygun H. D., H., Sensors and Actuators B: Chemical, 202 (2014) 448-453.

[98] Wagner C., Muilenber G.E., Riggs W.M., Davis L.E., Moulder J.F., Handbook of X-ray Photoelectron Spectroscopy, Perkin-Elmer, Physical Electronic Division, Eden Prairie, Minnesota, 1979.

[99] He L., Liang B., Li L., Yang X., Huang Y., Wang A., Wang X., Zhang T., ACS Catal. 5 (2015) 1623–1628.

[100] A.J. Bard, R. Parsons, J. Jordan, Standard Potentials in Aqueous Solution, Marcel Dekker Inc., New York, 1985.

[101] Ma Y.-Y, Wu C.-X., Feng X.-J., Tan H.-Q., Yan L.-K., Liu Y., Kang Z.-H., Wang E.-B., Li Y.-G., Energy Environ. Sci., 10 (2017) 788-798.

[102] Cao B., Veith G. M., Neuefeind J. C., Adzic R. R., Khalifah P. G., J. Am. Chem. Soc. 135 (2013) 19186-19192.

[103] Sadiek I. M., Mohammed A. M., El-Shakre M. E., Awad I. M., El-Deab M. S., El-Anadouli B. E., Int. J. Electrochem. Sci., 7 (2012) 3350-3361.

[104] Xiong D., Wang X., Li W., Liu L., RSC Chem. Commun., 52 (2016) 8711-8714.

[105] Yan K. L., Shang X., Gao W. K., Dong B., Li X., Chi J. Q., Liu Y. R., Chai Y. M., Liu C.G., J. Alloys Compd., 719 (2017) 314-321.

APPENDICES

APPENDIX A

TEM IMAGES OF Ru^0/TiO_2, Ru^0/ZrO_2, Ru^0/HfO_2 CATALYSTS

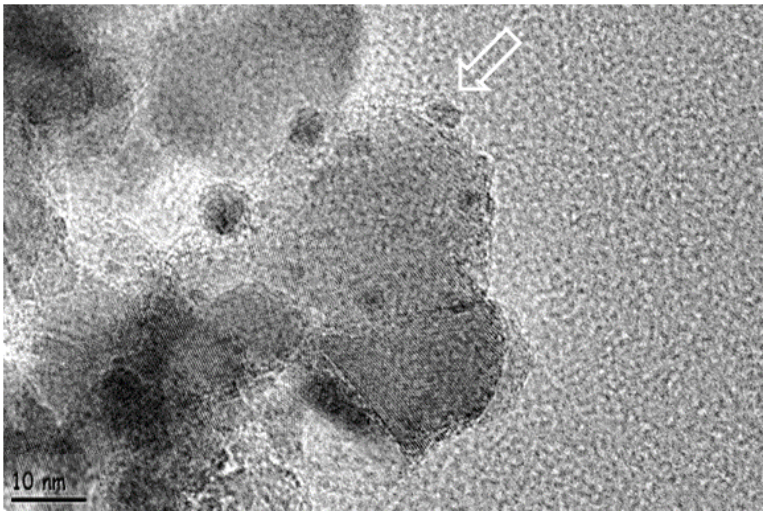

Figure A.1. TEM image of Ru^0/TiO_2 (1.20% wt. Ru), scale bar equals to 10.0 nm.

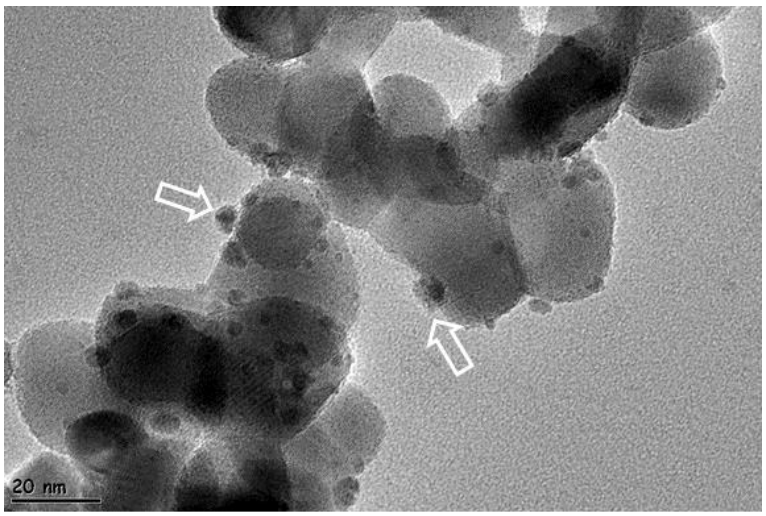

Figure A.2. TEM image of Ru^0/ZrO_2 (1.41% wt. Ru), scale bar equals to 20.0 nm.

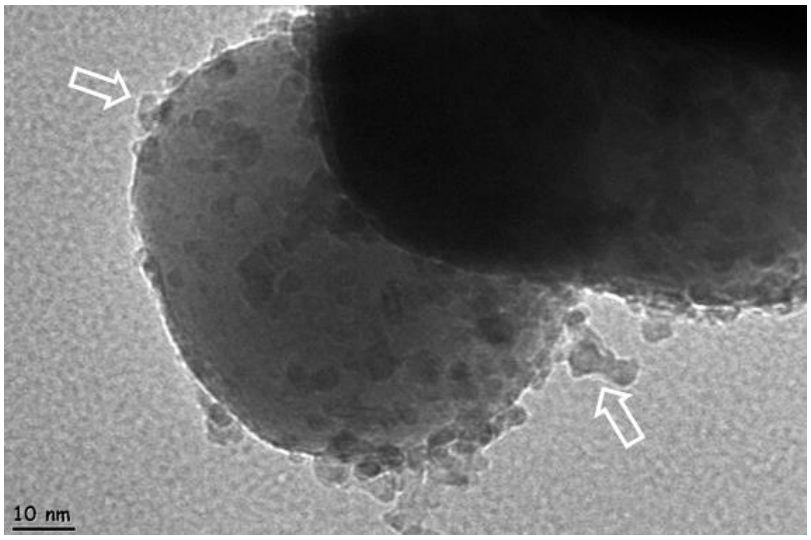

Figure A.3. TEM image of Ru^0/HfO_2 (2.00% wt. Ru), scale bar equals to 10.0 nm.

APPENDIX B

XPS SPECTRUM OF Ru^0/CeO_2 (1.86% wt. Ru)

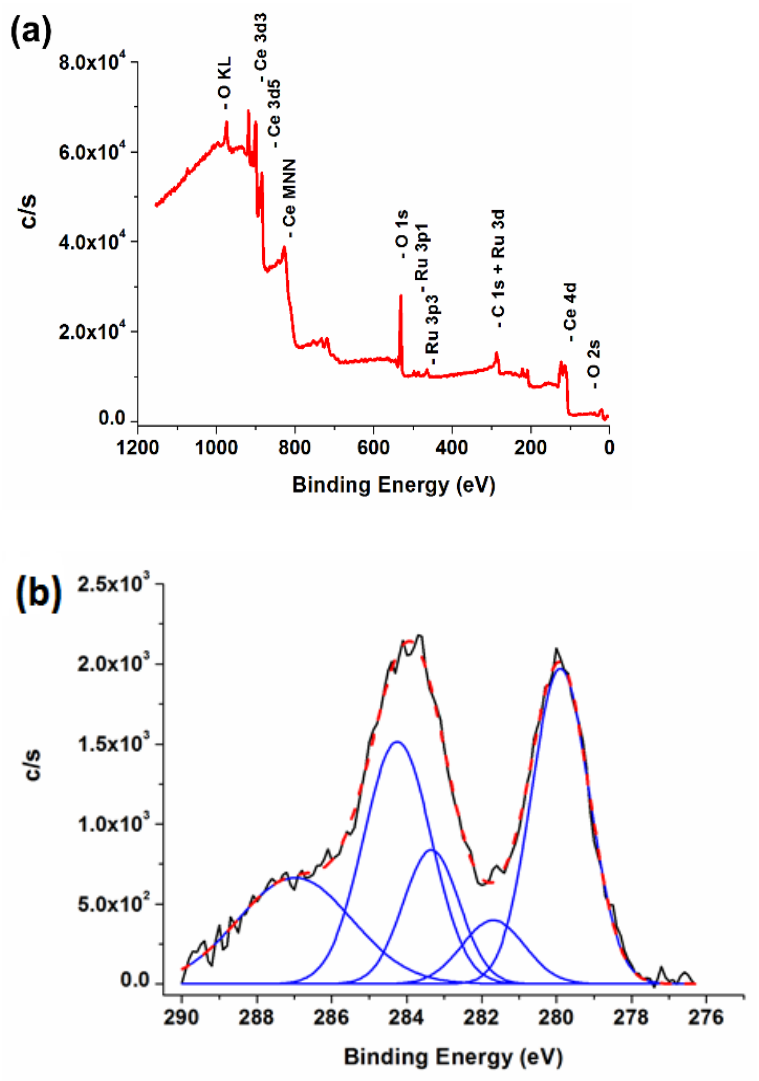

Figure B.1. (a) X-ray photoelectron (XPS) spectrum of Ru^0/CeO_2 with a 1.86% wt. Ru, **(b)** the high resolution scan and deconvolution of Ru 3d band.

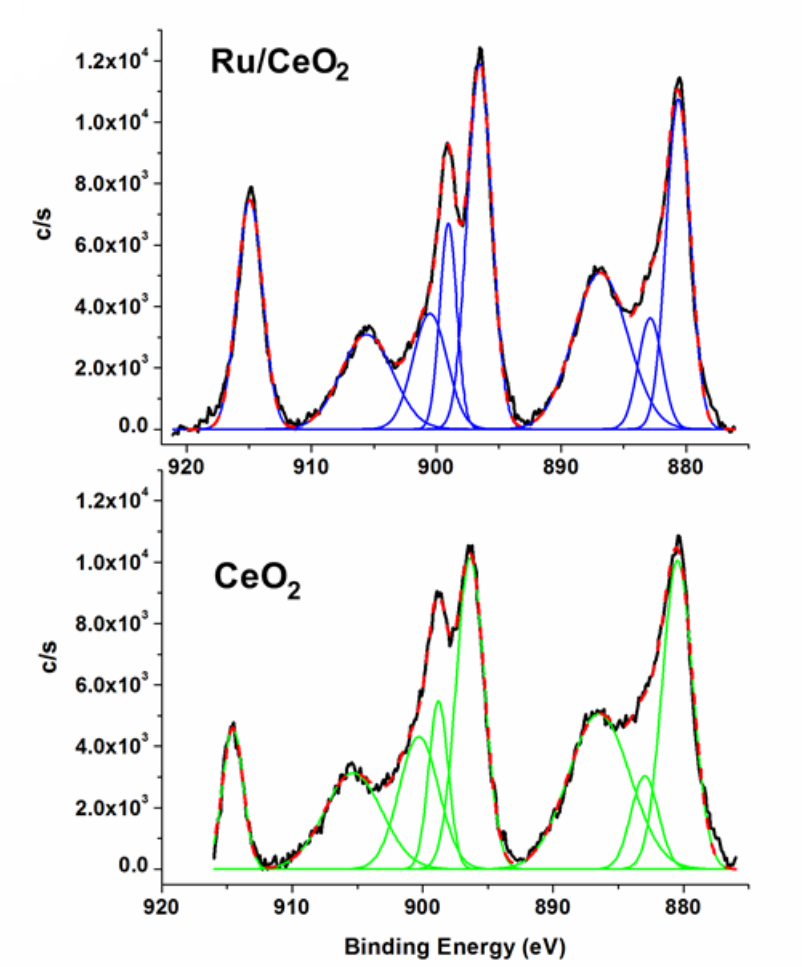

Figure B.2. XPS scan and deconvolution of Ce 3d bands of CeO_2 and Ru^0/CeO_2 (1.86% wt. Ru).